Developing the Coupling of the Mechanical to the Electrical and Calcium Systems in a Heart Cell

REU Site: Interdisciplinary Program in High Performance Computing

Kristen Deetz[1], Nygel Foster[2], Darius Leftwich[2], Chad Meyer[3], Shalin Patel[4], Graduate assistant: Carlos Barajas[5], Faculty mentor: Matthias K. Gobbert[5], and Client: Zana Coulibaly[6]

[1]Department of Mathematics, Eastern University,
[2]Department of Computer Science and Electrical Engineering, UMBC,
[3]Department of Mathematics, University of Pittsburgh,
[4]Department of Computer Science and Mathematical Science, Kean University,
[5]Department of Mathematics and Statistics, UMBC,
[6]Department of Pharmacology, University of California, Davis

Technical Report HPCF–2017–15, hpcf.umbc.edu > Publications

Abstract

As the leading cause of death in the United States, heart disease has become a principal concern in modern society. Cardiac arrhythmias can be caused by a dysregulation of calcium dynamics in cardiomyocytes. Calcium dysregulation, however, is not yet fully understood and is not easily predicted; this provides motivation for the subsequent research. Excitation-contraction coupling (ECC) is the process through which cardiomyocytes undergo contraction from an action potential. Calcium induced calcium release (CICR) is the mechanism through which electrical excitation is coupled with mechanical contraction through calcium signaling. The study of the interplay between electrical excitation, calcium signaling, and mechanical contraction has the potential to better our understanding of the regular functioning of the cardiomyocytes and help us understand how any dysregulation can lead to potential cardiac arrhythmias. ECC, of which CICR is an important part, can be modeled using a system of partial differential equations that link the electrical excitation, calcium signaling, and mechanical contraction components of a cardiomyocyte. We extend a previous model to implement a seven variable model that includes for the first time the mechanical component of the ECC. We conduct a parameter study to determine how the interaction of electrical and calcium systems can impact the cardiomyocyte's levels of contraction.

Key words. Heart disease, Heart cell, Cardiac arrhythmia, Excitation-contraction coupling, Calcium Induced Calcium Release.

1 Introduction

The leading cause of death in the United States is currently heart disease [11]. However, in order to continue searching for methods to combat heart disease, it is vital that the heart and its underlying processes are understood with greater depth. The importance of having a greater understanding of the heart provides the motivation for this research. The following research studies a single cardiac cell and uses a mathematical model in order to represent the electrical excitation, calcium signaling, and mechanical contraction of a cardiomyocyte. A seven variable partial differential equation model is used in order to represent the excitation-contraction coupling (ECC) occurring in the cardiomyocyte. This is concretely realized by calcium induced calcium release (CICR), which is the mechanism through which electrical excitation is coupled with mechanical contraction through calcium signaling.

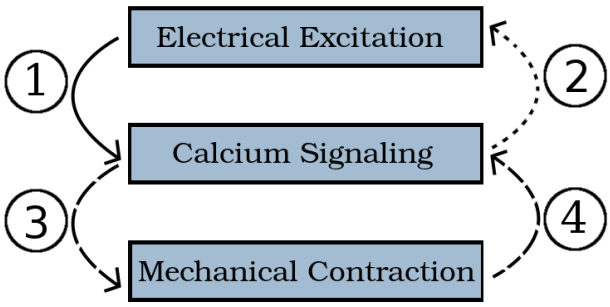

Figure 1.1: The three components of the model and their links labeled ① to ④.

The original model for CICR was introduced in [7, 9] with three variables and only included calcium signaling and extended in [8]. This original model comprises the heart of the Calcium Signaling component of the system indicated in Figure 1.1. The model was extended for the first time to include the Electrical Excitation component in Figure 1.1 in [1,2], which implemented a one-way interaction from electrical excitation to calcium signaling indicated by link ① in Figure 1.1. Studies with six variables in [3,4] extended the coupling to include a two-way cycle between electrical excitation and calcium signaling by incorporating both links ① and ② in Figure 1.1. This work studies seven variables through the introduction of the Mechanical Contraction component in Figure 1.1 by activating the links ③ and ④ in Figure 1.1. We note that [3, 4] introduced the formulation of the complete eight variable model, but studies that incorporate the mechanical system were not performed so far.

This report is organized as follows: Section 2 explains the physiological background behind the system being studied. Section 3 specifies the exact model with all equations, formulas, and parameter values of the seven variable model used in this work. Section 4 documents the approach to developing the implementation. Section 5 summarizes the numerical method used. Section 6 presents the complete results of two studies with different coupling strengths of the voltage to the cytosol calcium. Finally, Section 7 summarizes our conclusions.

2 Dynamics of a Cardiac Cell

In order to understand the electrical excitation, calcium signaling, and mechanical contraction cycle of a cardiomyocyte, it is important to first understand the basic structure of a cardiac cell. A cardiac cell takes the basic shape of a rectangle with T-tubules running along the sides of the cell. The muscle fibers of the cell run parallel with the contractile proteins, which allows for the contraction and relaxation of the cell, represented by links ③ and ④ in Figure 1.1. When observing Figure 2.1 (a), one can see that a cardiomyocyte contains a sacroplasmic reticulum (SR), which contains calcium ions and calsequestrin (CSQ). The SR contains calcium release units (CRUs), which calcium is released through from the SR to the cytosol of the cell. Sparking, or the scattered local simultaneous openings of CRUs, occurs when the concentration of calcium is high enough in the cytosol that the CRUs begin to open. In order to see the calcium more easily during experiments, a dye is mixed in the cell's cytosol that will bind to the calcium.

At the top of Figure 2.1 (a), the sodium-calcium electrical exchanger is labeled as NCX. The job of the NCX is to bring three sodium ions into the cell while also pushing out one calcium ion. Link 2 in Figure 1.1 represents this feedback of calcium leaving the cell. The calcium concentration inside

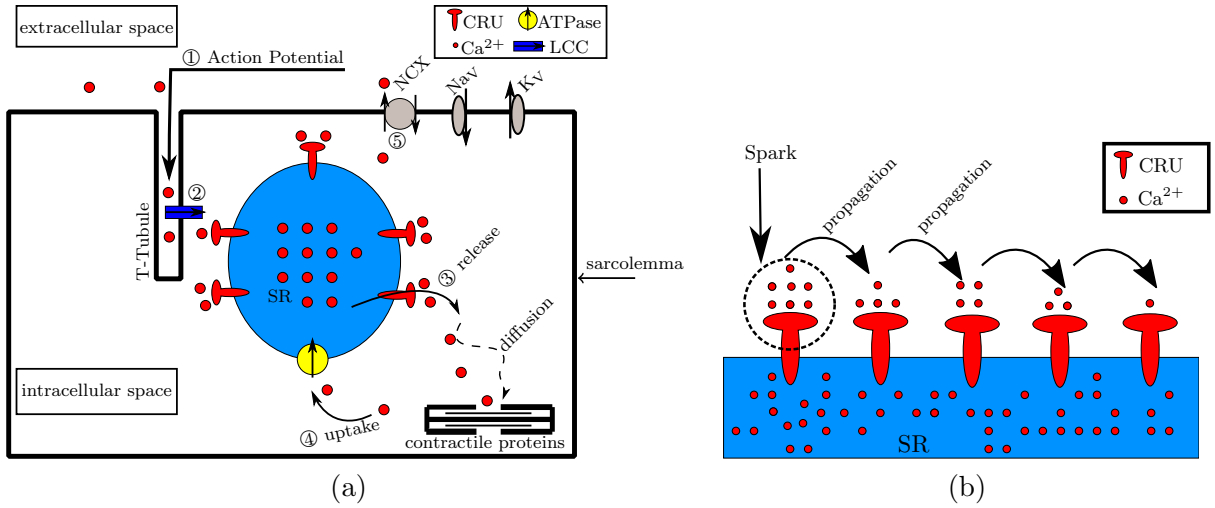

Figure 2.1: (a) Calcium wave triggering. (b) Cellular space.

the cytosol influences the electrical excitation of this cycle happening inside the cardiomyocyte. As the concentration of calcium in the cytosol begins to change, this causes depolarizations of the cell plasma membrane, which in turn causes action potential that leads to the opening of the L-type Calcium Channels (LCC). This process of action potential causes the LCC to open is the feedforward mechanism represented as link ① in Figure 1.1. This feedforward mechanism allows for the electrical excitation to influence the calcium concentration in the cytosol. The previously mentioned methods, represented by links ① and ②, lead to a two-way connection between the electrical excitation and calcium signaling occuring in the cardiac cell.

During the process of calcium release from the CRUs into the cytosol, there exists a spike in calcium concentration which can trigger local CRUs to open in addition to the possible cascading effect as Figure 2.1 (b) resembles. While there is still calcium in the SR, this wave can propagate, then calcium is replenished from an intracellular pump on the SR that acts as a source. Calcium induced calcium release is a behavior described as the process where calcium pours into the cytosol thus increasing the concentration and triggering another wave event within the cell. During calcium diffusion within the cytosol, it reacts with the other chemical species (fluorescent dye, fluoro-4, and tropomyosin contractile proteins).

The contractile proteins, tropomyosin, are responsible for the contraction and expansion of the cell's shape. These proteins are a composition of troponin, actin, myosin heads, and are attached to a sacromere. This sacromere, parallel to the tropomyosin, contracts when the myosin heads come in contact with the actin bridge; this happens when calcium binds to the troponin complex leaving the myosin heads free to converge on the bridge. Myosin contraction can be described as the physical process where the cell expands and contracts; when these contractions perform in unison with other cardiac cells, the corresponding section of the heart pulses. The first coupling between the calcium and the contractile nature of a heart cell is here; we can describe these chemical interactions as a feedforward process and can be represented by link ③ in Figure 1.1. The bridge-like structure deforms once calcium binds to the complex; this causes the bridge to hang onto the calcium longer. The increase in concentration in the cytosol as a feedback process is a result of the calcium being relinquished from the bridge; this process is represented by link ④ in Figure 1.1.

3 Model

This section details the seven variable model used in this work. It is a special case of the eight variable model fully established in [3]. The PDEs used in the implemented model are (3.1), (3.2) with $n_{sc} = 3$, (3.3), (3.4) with $n_{ss} = 0$, (3.12), and (3.13) yielding a total number of $n_s = 4+n_{sc}+n_{ss} = 7$ PDEs. The seven species of the model are: calcium in the cytosol $c(\mathbf{x}, t)$, a florescent dye $b_1^{(c)}(\mathbf{x}, t)$, a contractile protein (troponin) $b_2^{(c)}(\mathbf{x}, t)$, a contractile force $b_3^{(c)}(\mathbf{x}, t)$, calcium in the SR $s(\mathbf{x}, t)$, voltage $V(\mathbf{x}, t)$, and the potassium gating function $n(\mathbf{x}, t)$. Section 3.1 describes the calcium signaling portion of the model. Section 3.2 describes the electrical excitation that is connected to the calcium signaling in both the feedforward and feedback directions represented by link ① and link ② in Figure 1.1. Link ① from electrical system to the calcium dynamics was first established in [2], and link ② was established in [3]. Finally, Section 3.3 presents the mechanical contraction component that is also connected to the calcium signaling in both the feedback and feedforward directions represented by links ③ and ④ in Figure 1.1 and was established in [3].

3.1 Calcium Signaling

We start with a system of time-dependent, coupled, non-linear reaction diffusion equations

$$\frac{\partial c}{\partial t} = \nabla \cdot (D_c \nabla c) + \sum_{i=1}^{n_{sc}} R_i^{(c)} + \left(J_{CRU} + J_{leak} - J_{pump}\right) + \kappa\, J_{LCC} + \left(J_{m_{leak}} - J_{m_{pump}}\right), \quad (3.1)$$

$$\frac{\partial b_i^{(c)}}{\partial t} = \nabla \cdot (D_{b_i^{(c)}} \nabla b_i^{(c)}) + R_i^{(c)}, \quad i = 1, \ldots, n_{sc}, \quad (3.2)$$

$$\frac{\partial s}{\partial t} = \nabla \cdot (D_s \nabla s) + \sum_{j=1}^{n_{ss}} R_j^{(s)} - \gamma (J_{CRU} + J_{leak} - J_{pump}), \quad (3.3)$$

$$\frac{\partial b_j^{(s)}}{\partial t} = \nabla \cdot (D_{b_j^{(s)}} \nabla b_j^{(s)}) + R_j^{(s)}, \quad j = 1, \ldots, n_{ss}, \quad (3.4)$$

where $c(\mathbf{x}, t)$ and $s(\mathbf{x}, t)$ represent the concentrations of calcium in the cytosol and SR, respectively. The species $b_i^{(c)}(\mathbf{x}, t)$, $i = 1, \ldots, n_{sc}$, and $b_j^{(s)}(\mathbf{x}, t)$, $j = 1, \ldots, n_{ss}$, represent the concentration of each buffer species in the cytosol and SR, respectively. Table 3.1 collects the variables of the model with their units as well as their initial values. Table 3.2 contains the parameters in the PDEs of the calcium system with their values (if fixed) and units. The coefficients D_c, $D_{b_i^{(c)}}$, D_s, and $D_{b_j^{(s)}}$ are the diffusivity matrices for Ca^{2+} in the cytosol, buffer species i in the cytosol, Ca^{2+} in the SR, and buffer species j in the SR, respectively. While each buffer species programmatically possesses a diffusivity matrix (following the template of (3.2) and (3.4)), not all species are mobile; hence the diffusivity matrices for some species are zero matrices in Table 3.2.

The reaction terms $R_i^{(c)}$ and $R_j^{(s)}$ describe the reactions between calcium and the buffer species. They are the connections between (3.1) and (3.2), and between (3.3) and (3.4). More precisely,

$$R_i^{(c)} = -k^+_{b_i^{(c)}}\, c\, b_i^{(c)} + k^-_{b_i^{(c)}} \left(b_{i,total}^{(c)} - b_i^{(c)}\right), \quad i = 1, \ldots, n_{sc}, \quad (3.5)$$

model the reactions between cytosolic Ca^{2+} and each cytosolic buffer species, and

$$R_j^{(s)} = -k^+_{b_j^{(s)}}\, s\, b_j^{(s)} + k^-_{b_j^{(s)}} \left(b_{j,total}^{(s)} - b_j^{(s)}\right), \quad j = 1, \ldots, n_{ss}, \quad (3.6)$$

Table 3.1: Variables of the model and their initial conditions. The concentration unit M is shorthand for mol/L (moles per liter).

Variable	Definition	Values/Units
$\mathbf{x}$	spatial position variable (x, y, z)	μm
t	time variable	ms
n_{sc}	number of cytosol buffer species	3
n_{ss}	number of SR buffer species	0
$c(\mathbf{x}, t)$	calcium in the cytosol	μM
$b_1^{(c)}(\mathbf{x}, t)$	free flourescent dye in the cytosol	μM
$b_2^{(c)}(\mathbf{x}, t)$	free troponin in the cytosol	μM
$b_3^{(c)}(\mathbf{x}, t)$	inactive actin-myosin cross-bridges [X] in the cytosol	μM
$s(\mathbf{x}, t)$	calcium in the SR	μM
$V(\mathbf{x}, t)$	membrane potential (voltage)	mV
$n(\mathbf{x}, t)$	fraction of open potassium channels	0 to 1
c_0	basal cytosol calcium concentration	0.1 μM
s_0	initial SR calcium concentration	10,000 μM
$c(\mathbf{x}, 0)$	initial concentration of $c(\mathbf{x}, t)$	$c_0 = 0.1$ μM
$b_1^{(c)}(\mathbf{x}, 0)$	initial concentration of $b_1^{(c)}(\mathbf{x}, t)$	45.918 μM
$b_2^{(c)}(\mathbf{x}, 0)$	initial concentration of $b_2^{(c)}(\mathbf{x}, t)$	111.818 μM
$b_3^{(c)}(\mathbf{x}, 0)$	initial concentration of $b_3^{(c)}(\mathbf{x}, t)$	145.20 μM
$s(\mathbf{x}, 0)$	initial concentration of $s(\mathbf{x}, t)$	$s_0 = 10{,}000$ μM
$V(\mathbf{x}, 0)$	initial membrane potential (voltage) of $V(\mathbf{x}, t)$	-50 mV
$n(\mathbf{x}, 0)$	initial fraction of open potassium channels of $n(\mathbf{x}, t)$	0.1

model the reactions between SR Ca^{2+} and each SR buffer species.

In the cytosol, this work considers three buffer species ($n_{sc} = 3$): a fluorescent dye $b_1^{(c)}(\mathbf{x}, t)$, a contractile protein troponin $b_2^{(c)}(\mathbf{x}, t)$, and inactive actin-myosin cross-bridges $b_3^{(c)}(\mathbf{x}, t)$. The reaction model for $b_1^{(c)}(\mathbf{x}, t)$ is (3.5) with $i = 1$ above, but when involving the pseudo-mechanical dynamics of the cell, the reactions for $b_2^{(c)}(\mathbf{x}, t)$ and $b_3^{(c)}(\mathbf{x}, t)$ are in fact given by the modified reaction models (3.20) and (3.19), respectively. This is explained in detail in Section 3.3 below.

In the SR, this work does not consider a buffer species ($n_{ss} = 0$), so (3.6) will vanish eventually.

Note that in (3.5), ${b_i}^{(c)}$ is the amount of unbound buffer known as "free" buffer. The constant $b_{i,total}^{(c)}$ denotes the total bound and unbound calcium thus leaving the difference seen in (3.5) to be the bound calcium. Since the model uses no-flux boundary conditions, no buffer species escapes or enters the cell, thus we only need to track the "free" buffer species and use $b_{i,total}^{(c)} - {b_i}^{(c)}$ for the bound species.

The flux terms J_{CRU}, J_{leak}, and J_{pump} in (3.1) describe the calcium induced release of Ca^{2+} into the cytosol from the SR, the continuous leak of Ca^{2+} into the cytosol from the SR, and the pumping of Ca^{2+} back into the SR from the cytosol. The terms $J_{LCC}, J_{m_{leak}}$, and $J_{m_{pump}}$ describe the fluxes of calcium into and out of the cell via the plasma membrane. The coupling between (3.1) and (3.3) is achieved by the three flux terms shared by both.

More precisely, J_{LCC}, $J_{m_{leak}}$, and $J_{m_{pump}}$ in (3.1) describe the fluxes of calcium into and out of the cell via the plasma membrane. J_{pump} replenishes the calcium stores in the SR; it increases SR

calcium concentration by decreasing cytosol calcium concentration. J_{leak} is a continuous leakage of those SR calcium stores into the cytosol; it increases cytosol concentration by decreasing SR calcium concentration. The pump term

$$J_{pump}(c) \;=\; V_{pump}\left(\frac{c^{n_{pump}}}{K_{pump}^{n_{pump}} + c^{n_{pump}}}\right) \tag{3.7}$$

is thus a function of cytosol calcium $c(\mathbf{x}, t)$. The leak term J_{leak} is a constant defined by

$$J_{leak} \;=\; J_{pump}(c_0), \tag{3.8}$$

which balances $J_{pump}(c)$ at basal level $c_0 = 0.1\ \mu$M of cytosol calcium. The pump term J_{pump}, a function of cytosolic calcium $c(\mathbf{x}, t)$, consists of the maximum pump velocity V_{pump} multiplied against the relationship between $c(\mathbf{x}, t)$ and the pump sensitivity K_{pump}; the exponent n_{pump} refers to the Hill coefficient (quantifying the degree of cooperative binding) for the pump function. This has the practical effect of multiplying the maximum possible pump velocity against a number between 0 and 1, exclusive. J_{leak}, which continuously leaks calcium into the cytosol from the SR, is simply J_{pump} evaluated at the basal cytosolic calcium concentration $c_0 = 0.1\,\mu M$. As noted, J_{pump} has two roles, namely to balance J_{leak} in the absence of sparking, but also to balance J_{CRU} under conditions of active calcium release.

The term J_{CRU} in (3.1) is the Ca^{2+} flux into the cytosol from the SR via each individual point source at which a CRU has been assigned. The effect of all CRUs is modeled as a superposition such that

$$J_{CRU}(c, s, \mathbf{x}, t) \;=\; \sum_{\hat{\mathbf{x}} \in \Omega_s} \hat{\sigma}\, \frac{s(\mathbf{x}, t)}{s_0}\, \mathcal{O}(c, s)\, \delta(\mathbf{x} - \hat{\mathbf{x}}) \tag{3.9}$$

with

$$\mathcal{O}(c, s) \;=\; \begin{cases} 1 & \text{if } u_{rand} \le J_{prob}, \\ 0 & \text{if } u_{rand} > J_{prob}, \end{cases} \tag{3.10}$$

where

$$J_{prob}(c, s) = P_{max}\left(\frac{c^{n_{prob_c}}}{K_{prob_c}^{n_{prob_c}} + c^{n_{prob_c}}}\right)\left(\frac{s^{n_{prob_s}}}{K_{prob_s}^{n_{prob_s}} + s^{n_{prob_s}}}\right). \tag{3.11}$$

Here, the effect of each CRU is modeled as a product of three terms: (i) Similarly to how in J_{pump} the maximum pump rate is scaled against the concentration of available cytosol calcium, the maximum pump rate is scaled against the concentration of available cytosol calicum, the maximum rate of Ca^{2+} release $\hat{\sigma}$ is scaled here against the ratio of calcium concentration in the SR. (ii) Following the same pattern a maximum value multiplied against some scaling proportion between 0 and 1 the gating function $\mathcal{O}$ has the practical effect of "budgeting" the calcium SR stores such that when the stores are low, the given CRU becomes much less likely to open; each CRU is assigned a uniformly distributed random value, which is compared to the single value returned by the CRU opening probability J_{prob} to determine whether or not the given CRU will open. (iii) The Dirac delta distribution $\delta(\mathbf{x} - \hat{\mathbf{x}})$ models each CRU as a point source for calcium release, which is defined by requiring $\delta(\mathbf{x} - \hat{\mathbf{x}}) = 0$ for all $\mathbf{x} \neq \hat{\mathbf{x}}$ and $\int_{\mathbb{R}^3} \psi(\mathbf{x})\delta(\mathbf{x} - \hat{\mathbf{x}})\, d\mathbf{x} = \psi(\hat{\mathbf{x}})$ for any continuous function $\psi(\mathbf{x})$.

Table 3.2: Parameters for calcium signaling.

Variable	Definition	Values/Units
D_c	diffusivity matrix for $c(\mathbf{x},t)$	diag(0.15,0.15,0.3) μm^2/ms
$D_{b_1^{(c)}}$	diffusivity matrix for $b_1^{(c)}$	diag(0.01,0.01,0.02) μm^2/ms
$D_{b_2^{(c)}}$	diffusivity matrix for $b_2^{(c)}$	diag(0.00,0.00,0.00) μm^2/ms
$D_{b_3^{(c)}}$	diffusivity matrix for $b_3^{(c)}$	diag(0.00,0.00,0.00) μm^2/ms
D_s	diffusivity matrix for $s(\mathbf{x},t)$	diag(0.78,0.78,0.78) μm^2/ms
D_v	diffusivity matrix for $V(\mathbf{x},t)$	diag(0.00,0.00,0.00) μm^2/ms
D_n	diffusivity matrix for $n(\mathbf{x},t)$	diag(0.00,0.00,0.00) μm^2/ms
$R_i^{(c)}$	reactions of cytosol Ca^{2+} with buffers	μM/ms
$R_j^{(s)}$	reactions of SR Ca^{2+} with buffers	μM/ms
$k^+_{b_1^{(c)}}$	forward reaction coefficient for $b_1^{(c)}$	0.080 (μM ms)$^{-1}$
$k^+_{b_2^{(c)}}$	forward reaction coefficient for $b_2^{(c)}$	0.100 (μM ms)$^{-1}$
$k^+_{b_3^{(c)}}$	forward reaction coefficient for $b_3^{(c)}$	0.040 ms^{-1}
$k^-_{b_1^{(c)}}$	reverse reaction coefficient for $b_1^{(c)}$	0.090 ms^{-1}
$k^-_{b_2^{(c)}}$	reverse reaction coefficient for $b_2^{(c)}$	0.100 ms^{-1}
$k^-_{b_3^{(c)}}$	reverse reaction coefficient for $b_3^{(c)}$	0.010 ms^{-1}
$b^{(c)}_{1,total}$	total amount of $b_1^{(c)}$ in the cytosol	50 μM
$b^{(c)}_{2,total}$	total amount of $b_2^{(c)}$ in the cytosol	123 μM
$b^{(c)}_{3,total}$	total amount of $b_3^{(c)}$ in the cytosol	150 μM
γ	ratio of volume of cytosol to SR	14
J_{leak}	calcium leak from SR	0.3209684 μM/ms
J_{pump}	calcium transfer from cytosol to SR	μM/ms
V_{pump}	maximum pump rate	4 μM/ms
K_{pump}	pump sensitivity to Ca^{2+}	0.184 μM
n_{pump}	Hill coefficient for pump function	4.0
J_{CRU}	calcium flux from SR to cytosol via CRUs	μM/ms
$\mathcal{O}$	gating function for J_{CRU}	0 or 1
J_{prob}	probability of CRU opening	0 to 1
$\mathbf{x}_s$	three-dimensional vector for CRU location	μm
Δx_s, Δy_s, Δz_s	CRU spacings in x-, y-, z-directions	0.8, 0.8, 2.0 μm
$\hat{\sigma}$	maximum rate of release	200 μM μm^3/ms
$\delta(\mathbf{x}-\hat{\mathbf{x}})$	Dirac delta distribution	$1/\mu$m^3
u_{rand}	uniformly distributed random variable	0 to 1
P_{max}	maximum probability for release	0.3
K_{prob_c}	sensitivity of CRU to cytosol calcium	2 μM
n_{prob_c}	Hill coefficient for probability function	4
K_{prob_s}	sensitivity of CRU to SR calcium	550 μM
n_{prob_s}	Hill coefficient for probability function	4

3.2 Electrical Excitation

The membrane potential of the cell depends on both the cytosol calcium ion concentration and also on the cytosol potassium ion (K^+) concentration [5, 10]. While a complete description of the relationship between electrolytes and membrane potential is beyond the scope of this paper, note the ω term in (3.12) quantifies a dependence of V on c to complete the coupling from the chemical to the the electrical systems in link ② in Figure 1.1, after c in (3.1) already contains several terms that depend on V to implement link ① in Figure 1.1. Table 3.3 contains the variables and parameters for electrical excitation.

The Ca^{2+} conductance is much faster than the K^+ conductance, so the calcium conductance can be approximated as m_∞ or instantaneously steady-state at all times; the potassium conductance requires a separate description in (3.13)

$$\begin{aligned}\frac{\partial V}{\partial t} \;=\; \tau_v \,\frac{1}{C}\Big(& I_{\text{app}} - g_L(V - V_L) - g_{Ca}\, m_\infty(V)\,(V - V_{Ca}) - g_K\, n\,(V - V_K) \\ & - \omega\,(J_{m_{leak}} - J_{m_{pump}})\Big),\end{aligned} \tag{3.12}$$

$$\frac{\partial n}{\partial t} \;=\; \tau_v\, \lambda_n\, \cosh\left(\frac{V - V_3}{2V_4}\right)\,\big(n_\infty(V) - n\big) \tag{3.13}$$

with

$$m_\infty(V) = \frac{1}{2}\left(1 + \tanh\left(\frac{V - V_1}{V_2}\right)\right), \tag{3.14}$$

$$n_\infty(V) = \frac{1}{2}\left(1 + \tanh\left(\frac{V - V_3}{V_4}\right)\right). \tag{3.15}$$

The connection between (3.1) and (3.12), link ① in Figure 1.1, the link from the electrical system to the calcium system, comes through

$$J_{LCC} \;= \frac{\tau_{flux}}{2F}\, S\, g_{Ca}\, m_\infty(V)\,(V - V_{Ca}), \tag{3.16}$$

the only calcium flux term to involve voltage. Note the parameter κ in (3.1), which is an external scaling factor for J_{LCC} rather than an intrinsic physiological component; if the value of κ is set to 0, the connection, link ① in Figure 1.1, is effectively switched off and the calcium dynamics are then modeled as though voltage were not involved. The surface area, S, of the cell is included in light of the fact that J_{LCC} describes the influx of calcium through L-type calcium channels (LCCs), which are present in the enclosing plasma membrane of the cell: the surface area of the cell is the surface area of the membrane.

We model the effect of cytosol calcium concentration on voltage by treating the calcium efflux term ($J_{m_{pump}} - J_{m_{leak}}$) as equivalent to the sodium-calcium exchanger current: we are thus able to describe the current generated by the sodium-calcium exchange as a function of simple calcium loss.

The individual components of the calcium efflux term are near-duplicates in form of the earlier J_{pump} and J_{leak} functions in (3.7) and (3.8), respectively. As J_{pump} described the removal of calcium from the cytosol and its transfer into SR stores,

$$J_{m_{pump}}(c) \;=\; V_{m_{pump}}\,\left(\frac{c^{n_{m_{pump}}}}{K_{m_{pump}}^{n_{m_{pump}}} + c^{n_{m_{pump}}}}\right) \tag{3.17}$$

describes the removal of calcium from the cytosol and its transfer to outside the cell across the membrane. The leak term J_{leak} described a gradual leak of calcium into the cytosol from the SR, while J_{CRU} described an abrupt, high-concentration (high relative to the leak) release of calcium into the cytosol from the SR. Similarly,

$$J_{m_{leak}} \;=\; J_{m_{pump}}(c_0) \tag{3.18}$$

describes a gradual leak of calcium into the cytosol from outside the cell via the plasma membrane, while J_{LCC} describes a sudden spike of calcium release into the cytosol via the LCCs.

The model connects the chemical system to the electrical system, link ② in Figure 1.1, via the inclusion of the current generated by calcium leaving the cell via $J_{m_{pump}}$ and $J_{m_{leak}}$, which directly affects the voltage. We collect and incorporate these as a single term, the calcium efflux $(J_{m_{pump}} - J_{m_{leak}})$, and use ω in (3.12) as a parameter for feedback strength in link ② in Figure 1.1, which is a scaling factor with the same essential function as κ in link ① in Figure 1.1 from (3.1): if it is set to 0, the only terms of (3.12) which depend on the cytosolic calcium concentration drop out, and the connection from calcium signaling to electrical excitation is severed.

3.3 Pseudo-Mechanical Contraction

The links ③ and ④ in Figure 1.1 provide feedback and feedforward terms for the contractile dynamics. We describe this as "pseudo-mechanical" because the domain itself is unchanged; in our model, the physical dimensions of the cell and the locations of the CRUs do not alter. We instead model the contraction via the proportion of contractile proteins which have bound to calcium and changed shape as a result, which generates the force required for cell contraction. Table 3.3 contains the variables and parameters for pseudo-mechanical contraction.

The contractile proteins in question, though considered as a single species, are the combination of actin and myosin when linked via cross-bridges. This linkage is made possible by Ca^{2+} binding to troponin, the cytosol buffer species $b_2^{(c)}(\mathbf{x},t)$: it is this binding that allows the actin-myosin cross-bridges to form. The cytosol species, $b_3^{(c)}(\mathbf{x},t)$, describes these actin-myosin cross-bridges and constructs a third cytosol reaction term

$$R_{b_3}^{(c)} \;=\; -\,k^{+}_{b_3^{(c)}} \left(\frac{b_{2,total}^{(c)} - b_2^{(c)}}{b_{2,total}^{(c)}} \right)^2 b_3^{(c)} + k^{-}_{b_3^{(c)}} \,(b_{3,total}^{(c)} - b_3^{(c)}). \tag{3.19}$$

Notice that this is not the same as the generic pattern for buffer species reaction terms from the initial model. There is no immediately clear dependence on cytosolic calcium $c(\mathbf{x},t)$. However, while $c(\mathbf{x},t)$ is not explicitly included, it is present in the proportion involving troponin, $b_3^{(c)}(\mathbf{x},t)$, which itself depends explicitly on cytosol calcium levels; $R_{b_3}^{(c)}$, like the other two reaction equations, does in fact depend on cytosol calcium concentration.

When troponin binds to Ca^{2+}, the protein as a whole, as noted, changes shape: not only does this allow actin-myosin cross-bridges to form, but it also traps the calcium in its connection to the troponin so that the disassociation rate decreases dramatically. To account for this, the shortening factor ε describes how the separation of troponin and calcium has been physically, not chemically, impaired. Note, again, that $R_{b_2}^{(c)}$ remains a function of cytosol calcium concentration $c(\mathbf{x},t)$ by its equation

$$R_{b_2}^{(c)} \;=\; -\,k^{+}_{b_2^{(c)}}\, c\, b_2^{(c)} + k^{-}_{b_2^{(c)}} \left(b_{2,total}^{(c)} - b_2^{(c)} \right) \frac{1}{\varepsilon} \tag{3.20}$$

Table 3.3: Variables and parameters for electrical excitation and mechanical contraction with base units of mho = $(s^3A^2)/(kgm^2)$ and F = $(s^4A^2)/(kgm^2)$.

Variable	Definition	Values/Units
τ_v	scaling factor to fit action potential duration in voltage equation	0.1 μM μm^3/ms
τ_{flux}	scaling factor to fit action potential duration in J_{LCC} equation	0.1
V_1	potential at which $m_\infty = 0.5$	-1.0 mV
V_2	reciprocal of slope of voltage dependence of m_∞	15.0 mV
V_3	potential at which $n_\infty = 0.5$	10.0 mV
V_4	reciprocal of slope of voltage dependence of n_∞	14.5 mV
V_L	equilibrium potential for leak conductance	-50 mV
V_{Ca}	equilibrium potential for Ca^{2+} conductance	100 mV
V_K	equilibrium potential for K^+ conductance	-70 mV
C	membrane capacitance	20 μF/cm^2
I_{app}	applied current	50 μA/cm^2
g_L	maximum/instantaneous conductance for leak	2 mmho/cm^2
g_{Ca}	maximum/instantaneous conductance for Ca^{2+}	4 mmho/cm^2
g_K	maximum/instantaneous conductance for K^+	8 mmho/cm^2
m_∞	fraction of open calcium channels at steady state	0 to 1
n_∞	fraction of open potassium channels at steady state	1
λ_n	maximum rate constant for opening of K^+ channels	0.1 ms^{-1}
J_{LCC}	influx of calcium into cell via L-type calcium channels	μM/ms
S	surface area of the cell	3604.48 μm
F	Faraday constant	95484.56 C/mol
κ	scaling factor of J_{LCC}	0.01 or 0.1
ω	feedback strength (scaling factor) for Ca^{2+} efflux	μA ms/μM cm^2
$J_{m_{leak}}$	leak of calcium out from cell via L-type calcium channels	0.1739493 μM/ms
$J_{m_{pump}}$	pump of calcium out from cell via L-type calcium channels	μM/ms
$V_{m_{pump}}$	maximum pump rate	2 μM/ms
$n_{m_{pump}}$	membrane pump Hill coefficient	4
$K_{m_{pump}}$	membrane pump Ca^2+ sensitivity	0.18
$[XB]_0$	initial concentration of active cross-bridges	142.6805 μM
ε	shortening factor	0 to 1
F_{max}	maximum force generated by actin-myosin crossbridges	10 μN
k_s	stiffness of actin filament	0.025 N/m

with

$$\varepsilon \;=\; \exp\left(F_{max}\,k_s\,\left(\frac{b_{3,total}^{(c)} - b_3^{(c)} - [XB]_0}{b_{3,total}^{(c)} - [XB]_0}\right)\right) \tag{3.21}$$

and

$$[XB]_0 = b_{3,total}^{(c)} - b_3^{(c)}(\mathbf{x}, 0). \tag{3.22}$$

This shortening factor ε links ③ and ④ in Figure 1.1. It refers back to the concentration of $b_3^{(c)}(\mathbf{x}, t)$, the actin-myosin cross-bridges, and to the force that their linkage generates. It is scaled

by the maximum possible contractile force F_{max}, the actin stiffness k_s, and the proportion of active to inactive actin-myosin cross-bridges.

The force in the cell is generated by the bound cross-bridge. While assuming a linear relationship between the force that the bound cross bridge produces and the concentration of the bound cross-bridge, this force can be represented by the following equation:

$$F = F_{max} \frac{(b_{3,total}^{(c)} - b_3^{(c)}) - (b_{3,total}^{(c)} - b_3^{(c)}(\mathbf{x}, 0))}{b_{3,total}^{(c)} - (b_{3,total}^{(c)} - b_3^{(c)}(\mathbf{x}, 0))}. \tag{3.23}$$

Like ω and κ, the factor ε is our point of control over the linkage between systems: if the argument of the exponential function is 0, the overall value simply turns to 1, and $R_{b_2}^{(c)}$ in (3.20) reverts to its earlier form (3.5) with $i = 2$.

These two reaction terms (3.19) and (3.20) connects the three components of our model. The calcium signaling is linked to the pseudo-mechanical contraction through the cross-bridge term, and the pseudo-mechanical contraction is in turn connected to the calcium signaling through the inclusion of the cytosol calcium concentration in the modified reaction equation for troponin. Thus all links ①, ②, ③, and ④ in Figure 1.1 are established, and thus the three systems of the model are fully linked.

3.4 Initial and Boundary Conditions

The concentration of cytosol calcium $c(\mathbf{x}, 0)$ is initialized to its basal level $c_0 = 0.1$ μM throughout the cell.

The initial values of all three cytosol buffer species $b_i^{(c)}(\mathbf{x}, 0)$, $i = 1, 2, 3$, in the model are chosen throughout the cell such that their reaction rates $R_i^{(c)} = 0$ when cytosol calcium is at basal level. Thus, it is not reactions that will prompt changes in the simulations after the initial time.

Specifically, $b_1^{(c)}(\mathbf{x}, 0)$ is calculated by setting $R_i^{(c)}$ with $i = 1$ in (3.5) to 0, which gives with $c = c_0$

$$b_1^{(c)}(\mathbf{x}, 0) = \frac{k_{b_1^{(c)}}^{-} b_{1,total}^{(c)}}{k_{b_1^{(c)}}^{+} c_0 + k_{b_1^{(c)}}^{-}}. \tag{3.24}$$

Before setting $R_2^{(c)}$ to 0, note first that the shortening factor ε in (3.21) has value 1.0 initially. This results from the numerator in the $\exp(\cdot)$ being 0, since by definition $b_3^{(c)}(\mathbf{x}, 0) + [XB]_0 = b_{3,total}^{(c)}$, that is, the sum of $b_3^{(c)}$ at the initial time plus $[XB]_0$ equals their combined maximum. Thus, the modified $R_2^{(c)}$ in (3.20) collapses to (3.5) with $i = 2$, and solving $R_2^{(c)} = 0$ yields

$$b_2^{(c)}(\mathbf{x}, 0) = \frac{k_{b_2^{(c)}}^{-} b_{2,total}^{(c)}}{k_{b_2^{(c)}}^{+} c_0 + k_{b_2^{(c)}}^{-}}. \tag{3.25}$$

This equation involves again the basal level c_0, but does not involve $b_3^{(c)}$, hence it can be computed first.

In order to find the initial value of $b_3^{(c)}(\mathbf{x}, 0)$, we set $R_{b_3}^{(c)}$ from (3.19) to 0. With $b_2^{(c)}(\mathbf{x}, 0)$ computed first from (3.25) above, it can be used here and solving $R_{b_3}^{(c)} = 0$ leads then to the

computable formula

$$b_3^{(c)}(\mathbf{x},0) = \frac{k^-_{b_3^{(c)}} b^{(c)}_{3,total}}{k^+_{b_3^{(c)}} \left(\frac{b^{(c)}_{2,total} - b_2^{(c)}(\mathbf{x},0)}{b^{(c)}_{2,total}} \right)^2 + k^-_{b_3^{(c)}}}. \tag{3.26}$$

The definition $b_3^{(c)}(\mathbf{x},0) + [XB]_0 = b^{(c)}_{3,total}$ is then used to compute the value $[XB]_0 = b^{(c)}_{3,total} - b_3^{(c)}(\mathbf{x},0)$ for use in (3.21) throughout the simulation.

The value $s_0 = 10{,}000$ μM is chosen as the initial concentration for the store $s(\mathbf{x},0)$ of calcium in the SR throughout the cell. This choice represents a rather higher value for the store of calcium in the SR, so that this is not a limiting factor to CRU activation initially.

For the variables in the electrical part of the model, we use $V(\mathbf{x},0) = -50$ mV for the membrane potential and $n(\mathbf{x},0) = 0.1$ for the fraction of open potassium channels.

The model uses no-flow boundary conditions for all diffusive variable, thus containing the total number of molecules of each species inside the cell.

4 Implementation Details

This section explains the approach to developing the implementation in the code and documents choices.

4.1 Implementation of Reaction Terms

We begin by re-stating the $n_s = 4 + n_{sc} + n_{ss} = 7$ PDEs of the model, (3.1), (3.2) with $n_{sc} = 3$, (3.3), (3.4) with $n_{ss} = 0$, (3.12), and (3.13), as explained at the beginning of Section 3, in one group, while also still listing n_{sc} and n_{ss} without using their values of $n_{sc} = 3$ and $n_{ss} = 0$, as

$$\frac{\partial c}{\partial t} = \nabla \cdot (D_c \nabla c) + \sum_{i=1}^{n_{sc}} R_i^{(c)} + \big(J_{CRU} + J_{leak} - J_{pump}\big) + \kappa\, J_{LCC} + \big(J_{m_{leak}} - J_{m_{pump}}\big), \tag{4.1}$$

$$\frac{\partial b_i^{(c)}}{\partial t} = \nabla \cdot (D_{b_i^{(c)}} \nabla b_i^{(c)}) + R_i^{(c)}, \quad i = 1, \ldots, n_{sc}, \tag{4.2}$$

$$\frac{\partial s}{\partial t} = \nabla \cdot (D_s \nabla s) + \sum_{j=1}^{n_{ss}} R_j^{(s)} - \gamma (J_{CRU} + J_{leak} - J_{pump}), \tag{4.3}$$

$$\frac{\partial b_j^{(s)}}{\partial t} = \nabla \cdot (D_{b_j^{(s)}} \nabla b_j^{(s)}) + R_j^{(s)}, \quad j = 1, \ldots, n_{ss}, \tag{4.4}$$

$$\begin{aligned} \frac{\partial V}{\partial t} = \tau_v \frac{1}{C} \Big(& I_{\text{app}} - g_L (V - V_L) - g_{Ca}\, m_\infty(V)\, (V - V_{Ca}) - g_K\, n\, (V - V_K) \\ & - \omega\, (J_{m_{leak}} - J_{m_{pump}}) \Big), \end{aligned} \tag{4.5}$$

$$\frac{\partial n}{\partial t} = \tau_v\, \lambda_n\, \cosh\left(\frac{V - V_3}{2V_4} \right) \big(n_\infty(V) - n \big). \tag{4.6}$$

Now, we list the equations explicitly as seven PDEs, using concretely $n_{sc} = 3$ and $n_{ss} = 0$, which leads to (4.2) repeated three times for $i = 1, 2, 3$ and (4.4) to being dropped in

$$\frac{\partial c}{\partial t} = \nabla \cdot (D_c \nabla c) + \sum_{i=1}^{n_{sc}} R_i^{(c)} + \big(J_{CRU} + J_{leak} - J_{pump}\big) + \kappa\, J_{LCC} + \big(J_{m_{leak}} - J_{m_{pump}}\big), \tag{4.7}$$

$$\frac{\partial b_1^{(c)}}{\partial t} = \nabla \cdot (D_{b_1^{(c)}} \nabla b_1^{(c)}) + R_1^{(c)}, \tag{4.8}$$

$$\frac{\partial b_2^{(c)}}{\partial t} = \nabla \cdot (D_{b_2^{(c)}} \nabla b_2^{(c)}) + R_2^{(c)}, \tag{4.9}$$

$$\frac{\partial b_3^{(c)}}{\partial t} = \nabla \cdot (D_{b_3^{(c)}} \nabla b_3^{(c)}) + R_3^{(c)}, \tag{4.10}$$

$$\frac{\partial s}{\partial t} = \nabla \cdot (D_s \nabla s) + \sum_{j=1}^{n_{ss}} R_j^{(s)} - \gamma (J_{CRU} + J_{leak} - J_{pump}), \tag{4.11}$$

$$\frac{\partial V}{\partial t} = \tau_v \frac{1}{C}\Big(I_{\text{app}} - g_L(V - V_L) - g_{Ca}\, m_\infty(V)\,(V - V_{Ca}) - g_K\, n\,(V - V_K) - \omega\,(J_{m_{leak}} - J_{m_{pump}})\Big), \tag{4.12}$$

$$\frac{\partial n}{\partial t} = \tau_v\, \lambda_n \cosh\left(\frac{V - V_3}{2V_4}\right)\big(n_\infty(V) - n\big). \tag{4.13}$$

Here, we introduce $u^{(i)}$ for $i = 0, \ldots, 6$ — using 0-based numbering as in the programming language C — in the equation instead of the native variable names c, $b_1^{(c)}$, …, n to get

$$\frac{\partial u^{(0)}}{\partial t} = \nabla \cdot (D^{(0)} \nabla u^{(0)}) + r^{(0)}(u^{(j)}, \mathbf{x}, t) + J_{CRU}, \tag{4.14}$$

$$\frac{\partial u^{(1)}}{\partial t} = \nabla \cdot (D^{(1)} \nabla u^{(1)}) + r^{(1)}(u^{(j)}, \mathbf{x}, t), \tag{4.15}$$

$$\frac{\partial u^{(2)}}{\partial t} = \nabla \cdot (D^{(2)} \nabla u^{(2)}) + r^{(2)}(u^{(j)}, \mathbf{x}, t), \tag{4.16}$$

$$\frac{\partial u^{(3)}}{\partial t} = \nabla \cdot (D^{(3)} \nabla u^{(3)}) + r^{(3)}(u^{(j)}, \mathbf{x}, t), \tag{4.17}$$

$$\frac{\partial u^{(4)}}{\partial t} = \nabla \cdot (D^{(4)} \nabla u^{(4)}) + r^{(4)}(u^{(j)}, \mathbf{x}, t) - \gamma\, J_{CRU}, \tag{4.18}$$

$$\frac{\partial u^{(5)}}{\partial t} = r^{(5)}(u^{(j)}, \mathbf{x}, t) \tag{4.19}$$

$$\frac{\partial u^{(6)}}{\partial t} = r^{(6)}(u^{(j)}, \mathbf{x}, t). \tag{4.20}$$

with

$$r^{(0)}(u^{(j)},\mathbf{x},t) \;=\; \sum_{i=1}^{n_{sc}} R_i^{(c)} + \big(J_{leak} - J_{pump}\big) + \kappa\, J_{LCC} + \big(J_{m_{leak}} - J_{m_{pump}}\big), \tag{4.21}$$

$$r^{(1)}(u^{(j)},\mathbf{x},t) \;= R_1^{(c)}, \tag{4.22}$$

$$r^{(2)}(u^{(j)},\mathbf{x},t) \;= R_2^{(c)}, \tag{4.23}$$

$$r^{(3)}(u^{(j)},\mathbf{x},t) \;= R_3^{(c)}, \tag{4.24}$$

$$r^{(4)}(u^{(j)},\mathbf{x},t) \;=\; \sum_{j=1}^{n_{ss}} R_j^{(s)} - \gamma\,(J_{leak} - J_{pump}), \tag{4.25}$$

$$\begin{aligned} r^{(5)}(u^{(j)},\mathbf{x},t) \;=& \tau_v\,\frac{1}{C}\Big(I_{app} - g_L(V - V_L) - g_{Ca}\,m_\infty(V)\,(V - V_{Ca}) - g_K\,n\,(V - V_K) \\ & - \omega\,(J_{m_{leak}} - J_{m_{pump}})\Big), \end{aligned} \tag{4.26}$$

$$r^{(6)}(u^{(j)},\mathbf{x},t) \;=\; \tau_v\,\lambda_n\,\cosh\left(\frac{V - V_3}{2V_4}\right)\,\big(n_\infty(V) - n\big). \tag{4.27}$$

or explicitly

$$\begin{aligned} r^{(0)} =& R_1^{(c)}(u^{(0)},u^{(1)}) + R_2^{(c)}(u^{(0)},u^{(2)},u^{(3)}) + R_3^{(c)}(u^{(2)},u^{(3)}) \\ & + (J_{leak} - J_{pump}(u^{(0)})) + \kappa\, J_{LCC}(u^{(5)}) + \big(J_{m_{leak}} - J_{m_{pump}}(u^{(0)})\big), \end{aligned} \tag{4.28}$$

$$r^{(1)} = R_1^{(c)}(u^{(0)},u^{(1)}) = -k^+_{b_1^{(c)}}\,u^{(0)}\,u^{(1)} + k^-_{b_1^{(c)}}\,\big(b^{(c)}_{1,total} - u^{(1)}\big), \tag{4.29}$$

$$r^{(2)} = R_2^{(c)}(u^{(0)},u^{(2)},u^{(3)}) = -k^+_{b_2^{(c)}}\,u^{(0)}\,u^{(2)} + k^-_{b_2^{(c)}}\,\left(b^{(c)}_{2,total} - u^{(2)}\right)\,\frac{1}{\varepsilon(u^{(3)})}, \tag{4.30}$$

$$r^{(3)} = R_3^{(c)}(u^{(2)},u^{(3)}) = -k^+_{b_3^{(c)}}\,\left(\frac{b^{(c)}_{2,total} - u^{(2)}}{b^{(c)}_{2,total}}\right)^2\,u^{(3)} + k^-_{b_3^{(c)}}\,(b^{(c)}_{3,total} - u^{(3)}), \tag{4.31}$$

$$r^{(4)} = \;-\gamma\,(J_{leak} - J_{pump}(u^{(0)})), \tag{4.32}$$

$$\begin{aligned} r^{(5)} =& \tau_v\,\frac{1}{C}\Big(I_{app} - g_L(u^{(5)} - V_L) - g_{Ca}\,m_\infty(u^{(5)})\,(u^{(5)} - V_{Ca}) - g_K\,u^{(6)}\,(u^{(5)} - V_K) \\ & - \omega\,(J_{m_{leak}} - J_{m_{pump}}(u^{(0)}))\Big), \end{aligned} \tag{4.33}$$

$$r^{(6)} = \tau_v\,\lambda_n\,\cosh\left(\frac{u^{(5)} - V_3}{2V_4}\right)\,\big(n_\infty(u^{(5)}) - u^{(6)}\big). \tag{4.34}$$

These equations are implemented in the code using the above formulations as basis. To document and help develop the code, the following Tables 4.1, 4.2, and 4.3 document the translation of the mathematical variables and quantities to variables in the code.

Table 4.1: Variables of the model and their variable names in the code.

Variable	Definition	Variable Names in Code
$\mathbf{x}$	spatial position variable (x, y, z)	`x, y, z`
t	time variable	`t`
n_{sc}	number of cytosol buffer species	`nsc`
n_{ss}	number of SR buffer species	`nss`
$c(\mathbf{x}, t)$	calcium in the cytosol	`u[0]`
${b_1}^{(c)}(\mathbf{x}, t)$	free flourescent dye in the cytosol	`u[1]`
${b_2}^{(c)}(\mathbf{x}, t)$	free troponin in the cytosol	`u[2]`
${b_3}^{(c)}(\mathbf{x}, t)$	inactive actin-myosin cross-bridges [X] in the cytosol	`u[3]`
$s(\mathbf{x}, t)$	calcium in the SR	`u[4]`
$V(\mathbf{x}, t)$	membrane potential (voltage)	`u[5]`
$n(\mathbf{x}, t)$	fraction of open potassium channels	`u[6]`
c_0	basal cytosol calcium concentration	`uini[0]`
s_0	initial SR calcium concentration	`uini[4]`
$c(\mathbf{x}, 0)$	initial concentration of $c(\mathbf{x}, t)$	`uini[0]`
$b_1^{(c)}(\mathbf{x}, 0)$	initial concentration of $b_1^{(c)}(\mathbf{x}, t)$	`uini[1]`
$b_2^{(c)}(\mathbf{x}, 0)$	initial concentration of $b_2^{(c)}(\mathbf{x}, t)$	`uini[2]`
$b_3^{(c)}(\mathbf{x}, 0)$	initial concentration of $b_3^{(c)}(\mathbf{x}, t)$	`uini[3]`
$s(\mathbf{x}, 0)$	initial concentration of $s(\mathbf{x}, t)$	`uini[4]`
$V(\mathbf{x}, 0)$	initial membrane potential (voltage) of $V(\mathbf{x}, t)$	`uini[5]`
$n(\mathbf{x}, 0)$	initial fraction of open potassium channels of $n(\mathbf{x}, t)$	`uini[6]`

Table 4.2: Variables and parameters for calcium signaling and their variable names in the code.

Variable	Definition	Variable Names in Code
D_c	diffusivity matrix for $c(\mathbf{x},t)$	diag(`Dx[0],Dy[0],Dz[0]`)
$D_{b_1^{(c)}}$	diffusivity matrix for $b_1^{(c)}$	diag(`Dx[1],Dy[1],Dz[1]`)
$D_{b_2^{(c)}}$	diffusivity matrix for $b_2^{(c)}$	diag(`Dx[2],Dy[2],Dz[2]`)
$D_{b_3^{(c)}}$	diffusivity matrix for $b_3^{(c)}$	diag(`Dx[3],Dy[3],Dz[3]`)
D_s	diffusivity matrix for $s(\mathbf{x},t)$	diag(`Dx[4],Dy[4],Dz[4]`)
D_v	diffusivity matrix for $V(\mathbf{x},t)$	diag(`Dx[5],Dy[5],Dz[5]`)
D_n	diffusivity matrix for $n(\mathbf{x},t)$	diag(`Dx[6],Dy[6],Dz[6]`)
$R_i^{(c)}$	reactions of cytosol Ca^{2+} with buffers	—
$R_j^{(s)}$	reactions of SR Ca^{2+} with buffers	—
$k^+_{b_1^{(c)}}$	forward reaction coefficient for $b_1^{(c)}$	`kf[1]`
$k^+_{b_2^{(c)}}$	forward reaction coefficient for $b_2^{(c)}$	`kf[2]`
$k^+_{b_3^{(c)}}$	forward reaction coefficient for $b_2^{(c)}$	`kf[3]`
$k^-_{b_1^{(c)}}$	reverse reaction coefficient for $b_1^{(c)}$	`kb[1]`
$k^-_{b_2^{(c)}}$	reverse reaction coefficient for $b_2^{(c)}$	`kb[2]`
$k^-_{b_3^{(c)}}$	reverse reaction coefficient for $b_3^{(c)}$	`kb[3]`
$b^{(c)}_{1,total}$	total amount of $b_1^{(c)}(\mathbf{x},t)$ in the cytosol	`usbar[1]`
$b^{(c)}_{2,total}$	total amount of $b_2^{(c)}(\mathbf{x},t)$ in the cytosol	`usbar[2]`
$b^{(c)}_{3,total}$	total amount of $b_3^{(c)}(\mathbf{x},t)$ in the cytosol	`usbar[3]`
γ	ratio of volume of cytosol to SR	`srgamma`
J_{leak}	calcium leak from SR	`jleak`
J_{pump}	calcium transfer from cytosol to SR	—
V_{pump}	maximum pump rate	`vpump`
K_{pump}	pump sensitivity to Ca^{2+}	`kpump`
n_{pump}	Hill coefficient for pump function	`npump`
J_{CRU}	calcium flux from SR to cytosol via CRUs	—
$\mathcal{O}$	gating function for J_{CRU}	—
J_{prob}	probability of CRU opening	—
$\mathbf{x}_s$	three-dimensional vector for CRU location	`xs,ys,zs`
Δx_s, Δy_s, Δz_s	CRU spacings in x-, y-, z-directions	`dxs`, `dys`, `dzs`
$\hat{\sigma}$	maximum rate of release	`sigmahat`
$\delta(\mathbf{x}-\hat{\mathbf{x}})$	Dirac delta distribution	—
u_{rand}	uniformly distributed random variable	`urand`
P_{max}	maximum probability for release	`pmax`
K_{prob_c}	sensitivity of CRU to cytosol calcium	`kprob`
n_{prob_c}	Hill coefficient for probability function	`nprob`
K_{prob_s}	sensitivity of CRU to SR calcium	`kprobs`
n_{prob_s}	Hill coefficient for probability function	`nprobs`

Table 4.3: Variables and parameters for electrical excitation and mechanical contraction and their variable names in the code.

Variable	Definition	Variable Names in Code
τ_v	scaling factor to fit action potential duration in voltage equations	`vol_tau`
τ_{flux}	scaling factor to fit action potential duration in J_{LCC} equation	`flux_tau`
V_1	potential at which $m_\infty = 0.5$	`vol_1`
V_2	reciprocal of slope of voltage dependence of m_∞	`vol_2`
V_3	potential at which $n_\infty = 0.5$	`vol_3`
V_4	reciprocal of slope of voltage dependence of n_∞	`vol_4`
V_L	equilibrium potential for leak conductance	`vol_l`
V_{Ca}	equilibrium potential for Ca^{2+} conductance	`vol_ca`
V_K	equilibrium potential for K^+ conductance	`vol_k`
C	membrane capacitance	`mcap`
I_{app}	applied current	`Iapp_max`
g_L	maximum/instantaneous conductance for leak	`gl`
g_{Ca}	maximum/instantaneous conductance for Ca^{2+}	`gca`
g_K	maximum/instantaneous conductance for K^+	`gk`
m_∞	fraction of open calcium channels at steady state	`Minf`
n_∞	fraction of open potassium channels at steady state	`Ninf`
λ_n	maximum rate constant for opening of K^+ channels	`vol_lambda`
J_{LCC}	influx of calcium into cell via L-type calcium channels	—
S	surface area of the cell	`cell_SA`
F	Faraday constant	`FaradayC`
κ	scaling factor of J_{LCC}	not implemented
ω	feedback strength (scaling factor) for Ca^{2+} efflux	`feedbackStrength`
$J_{m_{leak}}$	leak of calcium out from cell via L-type calcium channels	`pmleak`
$J_{m_{pump}}$	pump of calcium out from cell via L-type calcium channels	—
$V_{m_{pump}}$	maximum pump rate	`pmvpump`
$n_{p_{pump}}$	membrane pump Hill coefficient	`pmnpump`
$K_{m_{pump}}$	membrane pump Ca^2+ sensitivity	`pmkpump`
$[XB]_0$	initial concentration of active cross-bridges	`XB_0`
ε	shortening factor	`shorteningFactor`
F_{max}	maximum force generated by actin-myosin crossbridges	`F_max`
k_s	stiffness of actin filament	`actinStiffness`

4.2 Jacobian Matrix of the Non-Linear Terms

Since the spatial discretization of a parabolic partial differential equation results in a system of stiff ODEs, an implicit time-stepping method is needed. Thus, at every time step, a system of non-linear equations needs to be solved by the Newton method. This method requires the Jacobian matrix consisting of the components $\partial r^{(i)}/\partial u^{(j)}$ of derivatives of the vector of non-linear terms $r^{(i)}$, $i = 0, \ldots, 6$, in (4.28)–(4.34), differentiated with respect to their arguments $u^{(j)}$, $j = 0, \ldots, 6$.

We compute all $\partial r^{(i)}/\partial u^{(j)}$, $0 \leq i, j < 7$, concretely here as follows.
Derivatives of $r^{(0)}(u^{(j)}, \mathbf{x}, t)$ with respect to $u^{(j)}$, $0 \leq j < 7$:

$$\frac{\partial r^{(0)}}{\partial u^{(0)}} = -k^{+}_{b_1^{(c)}}\, u^{(1)} - k^{+}_{b_2^{(c)}}\, u^{(2)} - \frac{dJ_{pump}(u^{(0)})}{du^{(0)}} - \frac{dJ_{m_{pump}}(u^{(0)})}{du^{(0)}}, \tag{4.35}$$

$$\frac{\partial r^{(0)}}{\partial u^{(1)}} = -k^{+}_{b_1^{(c)}}\, u^{(0)} - k^{-}_{b_1^{(c)}}, \tag{4.36}$$

$$\frac{\partial r^{(0)}}{\partial u^{(2)}} = -k^{+}_{b_2^{(c)}}\, u^{(0)} - k^{-}_{b_2^{(c)}}\, \frac{1}{\varepsilon(u^{(3)})} + \frac{2k^{+}_{b_3^{(c)}}}{b^{(c)}_{2,total}} \left(\frac{b^{(c)}_{2,total} - u^{(2)}}{b^{(c)}_{2,total}} \right), \tag{4.37}$$

$$\frac{\partial r^{(0)}}{\partial u^{(3)}} = k^{-}_{b_2^{(c)}} \left(b^{(c)}_{2,total} - u^{(2)} \right) \frac{F_{max}\, k_s}{b^{(c)}_{3,total} - [XB]_0} \frac{1}{\varepsilon(u^{(3)})} - k^{+}_{b_3^{(c)}} \left(\frac{b^{(c)}_{2,total} - u^{(2)}}{b^{(c)}_{2,total}} \right)^2 - k^{-}_{b_3^{(c)}}, \tag{4.38}$$

$$\frac{\partial r^{(0)}}{\partial u^{(4)}} = 0, \tag{4.39}$$

$$\frac{\partial r^{(0)}}{\partial u^{(5)}} = \kappa\, \frac{dJ_{LCC}(u^{(5)})}{du^{(5)}}, \tag{4.40}$$

$$\frac{\partial r^{(0)}}{\partial u^{(6)}} = 0, \tag{4.41}$$

Derivatives of $r^{(1)}(u^{(j)}, \mathbf{x}, t)$ with respect to $u^{(j)}$, $0 \leq j < 7$:

$$\frac{\partial r^{(1)}}{\partial u^{(0)}} = -k^{+}_{b_1^{(c)}}\, u^{(1)}, \tag{4.42}$$

$$\frac{\partial r^{(1)}}{\partial u^{(1)}} = -k^{+}_{b_1^{(c)}}\, u^{(0)} - k^{-}_{b_1^{(c)}}, \tag{4.43}$$

$$\frac{\partial r^{(1)}}{\partial u^{(2)}} = 0, \tag{4.44}$$

$$\frac{\partial r^{(1)}}{\partial u^{(3)}} = 0, \tag{4.45}$$

$$\frac{\partial r^{(1)}}{\partial u^{(4)}} = 0, \tag{4.46}$$

$$\frac{\partial r^{(1)}}{\partial u^{(5)}} = 0, \tag{4.47}$$

$$\frac{\partial r^{(1)}}{\partial u^{(6)}} = 0, \tag{4.48}$$

Derivatives of $r^{(2)}(u^{(j)}, \mathbf{x}, t)$ with respect to $u^{(j)}$, $0 \leq j < 7$:

$$\frac{\partial r^{(2)}}{\partial u^{(0)}} = -\, k^{+}_{b_2^{(c)}}\, u^{(2)}, \tag{4.49}$$

$$\frac{\partial r^{(2)}}{\partial u^{(1)}} = 0, \tag{4.50}$$

$$\frac{\partial r^{(2)}}{\partial u^{(2)}} = -\, k^{+}_{b_2^{(c)}}\, u^{(0)} - k^{-}_{b_2^{(c)}}\, \frac{1}{\varepsilon(u^{(3)})}, \tag{4.51}$$

$$\frac{\partial r^{(2)}}{\partial u^{(3)}} = k^{-}_{b_2^{(c)}}\, \left(b^{(c)}_{2,total} - u^{(2)}\right)\, \frac{F_{max}\, k_s}{b^{(c)}_{3,total} - [XB]_0}\, \frac{1}{\varepsilon(u^{(3)})}, \tag{4.52}$$

$$\frac{\partial r^{(2)}}{\partial u^{(4)}} = 0, \tag{4.53}$$

$$\frac{\partial r^{(2)}}{\partial u^{(5)}} = 0, \tag{4.54}$$

$$\frac{\partial r^{(2)}}{\partial u^{(6)}} = 0, \tag{4.55}$$

Derivatives of $r^{(3)}(u^{(j)}, \mathbf{x}, t)$ with respect to $u^{(j)}$, $0 \leq j < 7$:

$$\frac{\partial r^{(3)}}{\partial u^{(0)}} = 0, \tag{4.56}$$

$$\frac{\partial r^{(3)}}{\partial u^{(1)}} = 0, \tag{4.57}$$

$$\frac{\partial r^{(3)}}{\partial u^{(2)}} = \frac{2k^{+}_{b_3^{(c)}}}{b^{(c)}_{2,total}}\, \left(\frac{b^{(c)}_{2,total} - u^{(2)}}{b^{(c)}_{2,total}}\right) \tag{4.58}$$

$$\frac{\partial r^{(3)}}{\partial u^{(3)}} = -\, k^{+}_{b_3^{(c)}}\, \left(\frac{b^{(c)}_{2,total} - u^{(2)}}{b^{(c)}_{2,total}}\right)^2 - k^{-}_{b_3^{(c)}}, \tag{4.59}$$

$$\frac{\partial r^{(3)}}{\partial u^{(4)}} = 0, \tag{4.60}$$

$$\frac{\partial r^{(3)}}{\partial u^{(5)}} = 0, \tag{4.61}$$

$$\frac{\partial r^{(3)}}{\partial u^{(6)}} = 0, \tag{4.62}$$

Derivatives of $r^{(4)}(u^{(j)}, \mathbf{x}, t)$ with respect to $u^{(j)}$, $0 \leq j < 7$:

$$\frac{\partial r^{(4)}}{\partial u^{(0)}} = \gamma \, \frac{dJ_{pump}(u^{(0)})}{du^{(0)}}, \tag{4.63}$$

$$\frac{\partial r^{(4)}}{\partial u^{(1)}} = 0, \tag{4.64}$$

$$\frac{\partial r^{(4)}}{\partial u^{(2)}} = 0, \tag{4.65}$$

$$\frac{\partial r^{(4)}}{\partial u^{(3)}} = 0, \tag{4.66}$$

$$\frac{\partial r^{(4)}}{\partial u^{(4)}} = 0, \tag{4.67}$$

$$\frac{\partial r^{(4)}}{\partial u^{(5)}} = 0, \tag{4.68}$$

$$\frac{\partial r^{(4)}}{\partial u^{(6)}} = 0, \tag{4.69}$$

Derivatives of $r^{(5)}(u^{(j)}, \mathbf{x}, t)$ with respect to $u^{(j)}$, $0 \leq j < 7$:

$$\frac{\partial r^{(5)}}{\partial u^{(0)}} = \frac{\tau_v}{C} \, \omega \, \frac{dJ_{m_{pump}}(u^{(0)})}{du^{(0)}}, \tag{4.70}$$

$$\frac{\partial r^{(5)}}{\partial u^{(1)}} = 0, \tag{4.71}$$

$$\frac{\partial r^{(5)}}{\partial u^{(2)}} = 0, \tag{4.72}$$

$$\frac{\partial r^{(5)}}{\partial u^{(3)}} = 0, \tag{4.73}$$

$$\frac{\partial r^{(5)}}{\partial u^{(4)}} = 0, \tag{4.74}$$

$$\frac{\partial r^{(5)}}{\partial u^{(5)}} = -\frac{\tau_v}{C} \left(g_L + g_{Ca}\big(\frac{dm_\infty(u^{(5)})}{du^{(5)}}(u^{(5)} - V_{Ca}) + m_\infty(u^{(5)})\big) + g_K u^{(6)} \right), \tag{4.75}$$

$$\frac{\partial r^{(5)}}{\partial u^{(6)}} = -\frac{\tau_v}{C} \, g_K \, (u^{(5)} - V_K), \tag{4.76}$$

Derivatives of $r^{(6)}(u^{(j)}, \mathbf{x}, t)$ with respect to $u^{(j)}$, $0 \leq j < 7$:

$$\frac{\partial r^{(6)}}{\partial u^{(0)}} = 0, \tag{4.77}$$

$$\frac{\partial r^{(6)}}{\partial u^{(1)}} = 0, \tag{4.78}$$

$$\frac{\partial r^{(6)}}{\partial u^{(2)}} = 0, \tag{4.79}$$

$$\frac{\partial r^{(6)}}{\partial u^{(3)}} = 0, \tag{4.80}$$

$$\frac{\partial r^{(6)}}{\partial u^{(4)}} = 0, \tag{4.81}$$

$$\frac{\partial r^{(6)}}{\partial u^{(5)}} = \tau_v \, \lambda_n \, \left(\frac{1}{2V_4} \, \sinh\left(\frac{u^{(5)} - V_3}{2V_4} \right) \, \left(n_\infty(u^{(5)}) - u^{(6)} \right) + \cosh\left(\frac{u^{(5)} - V_3}{2V_4} \right) \, \frac{dn_\infty(u^{(5)})}{du^{(5)}} \right), \tag{4.82}$$

$$\frac{\partial r^{(6)}}{\partial u^{(6)}} = \, - \tau_v \, \lambda_n \cosh\left(\frac{u^{(5)} - V_3}{2V_4} \right) \tag{4.83}$$

with derivatives of auxiliary functions

$$\frac{dJ_{pump}(u^{(0)})}{du^{(0)}} = V_{pump} \, \frac{n_{pump} K_{pump}^{n_{pump}} (u^{(0)})^{n_{pump}-1}}{(K_{pump}^{n_{pump}} + (u^{(0)})^{n_{pump}})^2}, \tag{4.84}$$

$$\frac{dJ_{m_{pump}}(u^{(0)})}{du^{(0)}} = V_{m_{pump}} \, \frac{n_{m_{pump}} K_{m_{pump}}^{n_{m_{pump}}} (u^{(0)})^{n_{m_{pump}}-1}}{(K_{m_{pump}}^{n_{m_{pump}}} + (u^{(0)})^{n_{m_{pump}}})^2}, \tag{4.85}$$

$$\frac{d\varepsilon(u^{(3)})}{du^{(3)}} = \, - \frac{F_{max} \, k_s}{b_{3,total}^{(c)} - [XB]_0} \, \varepsilon(u^{(3)}), \tag{4.86}$$

$$\frac{dJ_{LCC}(u^{(5)})}{du^{(5)}} = \frac{\tau_{flux}}{2F} \, S \, g_{Ca} \, \left(\left(u^{(5)} - V_{Ca} \right) \, \frac{dm_\infty(u^{(5)})}{du^{(5)}} + m_\infty(u^{(5)}) \right), \tag{4.87}$$

$$\frac{dm_\infty(u^{(5)})}{du^{(5)}} = \frac{1}{2} \, \frac{1}{V_2} \, \left(\cosh^2\left(\frac{u^{(5)} - V_1}{V_2} \right) \right)^{-1}, \tag{4.88}$$

$$\frac{dn_\infty(u^{(5)})}{du^{(5)}} = \frac{1}{2} \, \frac{1}{V_4} \, \left(\cosh^2\left(\frac{u^{(5)} - V_3}{V_4} \right) \right)^{-1}. \tag{4.89}$$

5 Numerical Method

In order to do calculations for the CICR model, we need to solve the system of time-dependent parabolic partial differential equations (PDEs) specified in Section 3. The PDEs are coupled by several non-linear reaction, source, and other terms on the right-hand side of the PDEs. For the simulations in Section 6, we have the seven variables specified in Table 3.1, thus we have $n_s = 7$ coupled PDEs. The domain in our model is a hexahedron $\Omega = (-6.4, 6.4)\times(-6.4, 6.4)\times(-32.0, 32.0)$ in units of μm with isotropic CRU distribution that captures the key feature of the elongated shape of a heart cell.

We take a method of lines (MOL) approach to spatially discretize this model, with the finite volume method (FVM) as the spatial discretization with (N_x+1), (N_y+1), (N_z+1) control volumes in the x-, y-, z-coordinate directions, thus there are a total of $N = (N_x+1)\,(N_y+1)\,(N_z+1)$ control volumes. The simulations in Section 6 use $N_x = N_y = 32$ and $N_z = 128$. Applying this to the case of the $n_s = 7$ PDEs results in a large system of ordinary differential equations (ODEs) with $n_{eq} = n_s\,N = 983{,}367$ degrees of freedom (DOF) as size of the system that needs to be solved at every time step.

A MOL discretization of a diffusion-reaction equations with second-order spatial derivatives results in a stiff ODE system. The time step size restrictions, due to the CFL condition, are considered too severe to allow for explicit time-stepping methods. This necessitates the use of a sophisticated ODE solver such as the family of numerical differentiation formulas (NDFk). Stiff ODEs need an implicit ODE method, thus requiring the solution of a non-linear system at every time step. We use the Newton method as non-linear solver, and the linear system in each Newton step is solved by BiCGSTAB as the linear solver. Complete details of the numerical method can be found in [6, 12]. BiCGSTAB is a Krylov subspace method, which only require matrix-vector products with the system matrix, not the matrix itself. Thus, we can dramatically reduce memory usage by using a matrix-free implementation of the linear solver that does not store the system matrix, but provides the results of the matrix-vector product. The code with the NDFk method of orders $1 \le k \le 5$ requires then, including all auxiliary method vectors, the storage of only 17 arrays of significant size n_{eq}. Simulation times depend heavily on the number of time steps taken.

The implementation of this model is done in C using MPI to parallelize computations. Parallelization is accomplished through block-distribution all large arrays to all MPI processes with split along the z-direction. MPI commands such as `MPI_Isend` and `MPI_Irecv` are non-blocking point-to-point communication commands used to communicate the interface data between blocks between neighboring processes. The collective command `MPI_Allreduce` is used for the computation of scalar products and norms.

Runs were done on "maya" which is operated by the UMBC High Performance Computing Facility (HPCF). The current machine in HPCF is the distributed-memory cluster maya with over 300 nodes. The components used from the cluster are the 72 nodes with two eight-core 2.6 GHz Intel E5-2650v2 Ivy Bridge CPUs and 64 GB memory that include 19 hybrid nodes The nodes are connected by a high-speed quad-data rate (QDR) InfiniBand network typically used for research on parallel algorithms. All nodes are connected via InfiniBand to a central storage of more than 750 TB. On this machine the runs typically took between ten minutes and thirty minutes per run with the times being largely dependent on the parameters being used.

6 Results

This section shows the results of simulations for the seven variable model outlined in Section 3. Table 3.1 lists the variables used in the model, and Tables 3.2 and 3.3 list the parameter values used. Specifically, Subsections 6.1 and 6.2 consider different strengths of the linkage of the voltage system to the cytosol calcium by parameter κ in Equation (3.1): Subsection 6.1 considers a higher coupling strength of $\kappa = 0.1$, and Subsection 6.2 a lower coupling strength of 0.01.

6.1 Higher Coupling Strength $\kappa = 0.1$

This subsection contains Figures 6.1 through 6.9, based on simulations using the values in Tables 3.1, 3.2 and 3.3, and with coupling strength $\kappa = 0.1$.

Figure 6.1 (a) plots the voltage in mV measured at the center point of the cell against time in ms in order to show how the voltage changes over the 1,000 ms time period. The voltage is the driving force for all other events happening in the cell. Voltage is represented by Equation (3.12) and is responsible the electrical excitation component of the model in Figure 1.1. This excitation is communicated through the J_{LCC} term, whose strength is controlled by κ, in Equation (3.1).

The plots in Figure 6.2 display the locations of open calcium release units by a dot. The more blue dots that are visible, the more CRUs that are open at that specific time. At some times and for short periods of time, CRUs form patterns and initiate diffusion waves, but no sustained waves form that would move through the entire cell. When many blue dots are appearing in an unorganized uniformly distributed fashion across the cell domain, this represents spontaneous sparking within the cell. The opening of CRUs is controlled by the model in Equations (3.9)–(3.11). This model embodies the effect of Calcium Induced Calcium Release (CICR) into the cytosol in that a higher concentration of cytosol calcium increases the probability for a CRU to open in (3.11), and an open CRU in turn increases the cytosol calcium concentration through the term J_{CRU} in Equation (3.1). Notice that the original trigger for increasing cytosol calcium comes from the J_{LCC} term in Equation (3.1) controlled by the voltage.

Figure 6.3 shows a collection of isosurface plots for calcium concentration in the cytosol. An isosurface plot displays the surface in the three-dimensional cell, where the species concentration is equal to a critical value, stated in the caption of the figure, here 65 μM for the concentration of cytosol calcium $c(\mathbf{x}, t)$. Due to the connection with open CRUs through the effect of Calcium Induced Calcium Release, calcium concentration in the cytosol in Figure 6.3 is high in the same areas of the cell where the CRUs are open in Figure 6.2 at that time. The line scan in Figure 6.1 (c) shows the calcium concentration in the cytosol of the cell over time on a two-dimensional slice through the center of the cell. The small sparks of color amidst the blue demonstrate how calcium increases in that specific location at that specific time.

Figure 6.4 shows the concentration of the free fluorescent dye in the cytosol modeled by Equation (3.2) with $i = 1$. As evident by the plots, the amount of free dye in the cytosol increases as the total time increases.

Figure 6.5 displays the concentration of the free troponin in the cytosol modeled by Equation (3.20). The plots display higher concentrations of troponin with yellow.

Figure 6.6 represents the concentration of the inactive actin-myosin cross-bridges throughout the cell, modeled by Equation (3.19). The plots indicates that at locations and times of increased cytosol calcium concentrations in Figure 6.3, the concentration of the *inactive* bridges decreases in Figure 6.6, implying an increase in the *active* bridges. These values enter into the Equation (3.21) for the shortening factor ε, whose values decrease from the neutral value 1.0 in these conditions.

The plot of ε at the center of the cell in Figure 6.1 (b) shows this behavior and indicates the connection to mechanical contraction component in Figure 1.1.

The plots displaying the calcium concentration $s(\mathbf{x}, t)$ of the store in the SR are located in Figure 6.7. The store in the SR has an initial value of 10,000 μM. When comparing these plots to the plots of calcium in the cytosol in Figure 6.3, we can see that there is a relationship. As the calcium concentration in the cytosol increases, more CRUs open as seen in Figure 6.2, which releases more calcium from the SR into the cytosol, resulting in a decreased concentration of the store in the SR. This is the effect of the J_{CRU} term with a negative sign in Equation (3.3) for $s(\mathbf{x}, t)$ A decreased value of $s(\mathbf{x}, t)$ at a certain location is of interest, since this limits eventually the ability of the CRU at that location to open in (3.11) as well as limits the amount of calcium released through the CRU in (3.9). We notice that due to more spontaneous openings of CRUs in the right end of the cell, the store concentration shows a larger decrease there.

The voltage $V(\mathbf{x}, t)$ modeled by (3.12) is represented by isosurface plots in Figure 6.8. This provides a broader view of the entire cell, as opposed to the two-dimensional plot of voltage at the center of the cell in Figure 6.1 (a). We see that the behavior is analogous across the cell.

Figure 6.9 represents the gating function $n(\mathbf{x}, t)$ of the potassium channels in the cell modeled by (3.13). The gating function clearly shows a behavior that is aligned in time with the voltage.

Finally, Figure 6.1 (b) plots the shortening factor ϵ in (3.21) against time to show how the shortening factor is changing over time. After comparing Figure 6.1 (b) to Figure 6.1 (a), we can see that the shortening factor mirrors the voltage plot such that as voltage increases, the shortening factor decreases. Likewise, as the voltage decreases, the shortening factor increases. This shows that the voltage is the driving force between the contraction and relaxation of a heart cell.

6.2 Lower Coupling Strength $\kappa = 0.01$

This subsection contains Figures 6.10 through 6.18, based on simulations using the values in Tables 3.1, 3.2 and 3.3, and with coupling strength $\kappa = 0.01$.

After comparing Figures 6.1 (a) and 6.10 (a), there is no evident change between the voltage when $\kappa = 0.1$ versus when $\kappa = 0.01$.

When comparing Figures 6.3 and 6.12, as well as Figures 6.1 (c) and 6.10 (c), we can see that the calcium concentration in the cytosol is slightly more active when $\kappa = 0.01$ than when $\kappa = 0.1$.

It is also evident that there is a change in the mechanical component of the model with a change in the value of κ when looking at Figures 6.6 and 6.15. For example, when $\kappa = 0.01$, there are less inactive actin-myosin cross-bridges during a significant portion of the 1,000 milliseconds shown in Figure 6.15 than in Figure 6.6 for $\kappa = 0.1$. This is evident by an increase of blue sections in the plots in Figure 6.15 compared to Figure 6.6. This shows that more actin-myosin cross-bridges are becoming activated in the $\kappa = 0.01$ case.

We can also see differences between the calcium concentration in the store in the SR when $\kappa = 0.1$ versus when $\kappa = 0.01$, as evident by comparing Figures 6.7 and 6.16. For example, the SR displays a larger depletion of calcium at time $t = 500$ ms for $\kappa = 0.1$ in Figure 6.7 compared to $t = 500$ ms for $\kappa = 0.01$ in Figure 6.16. Differences continue to appear for various time steps between these two cases.

Finally, while the plots of the shortening factor over time look very similar for cases $\kappa = 0.1$ and $\kappa = 0.01$ in Figures 6.1 (b) and 6.10 (b), it is vital to note that these plots are not exactly the same. For example, when $\kappa = 0.1$, the shortening factor has a minimum of approximately 0.99657 as seen in Figure 6.1 (b), while when $\kappa = 0.01$, the shortening factor has a minimum of approximately 0.99973 as seen in Figure 6.10 (b).

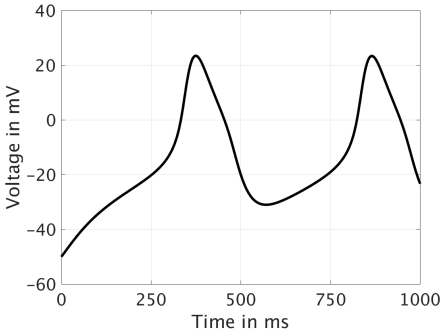

(a) Voltage over time.

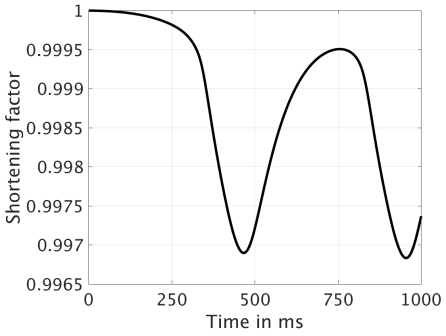

(b) Shortening factor over time.

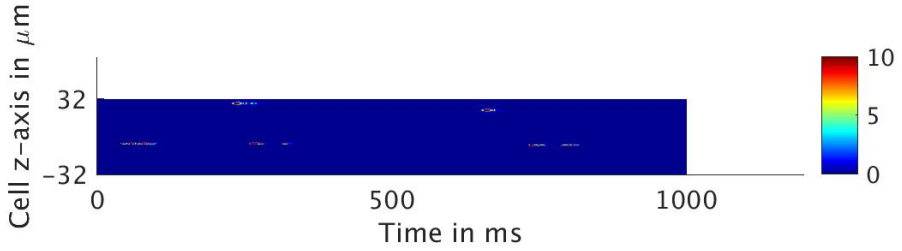

(c) Line scan.

Figure 6.1: Voltage, shortening factor, and line scan for $\kappa = 0.1$.

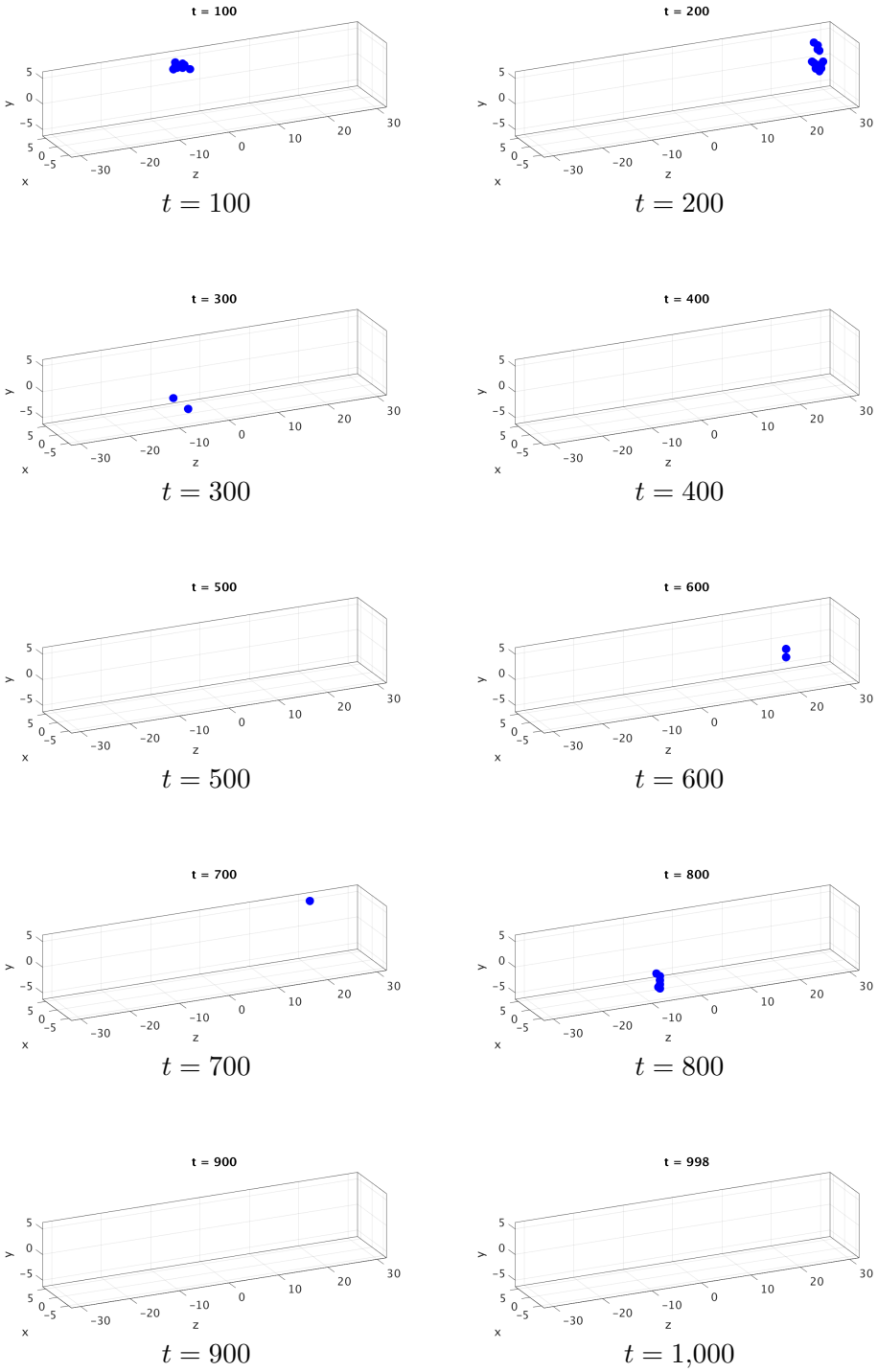

Figure 6.2: Open calcium release units throughout the cell for $\kappa = 0.1$.

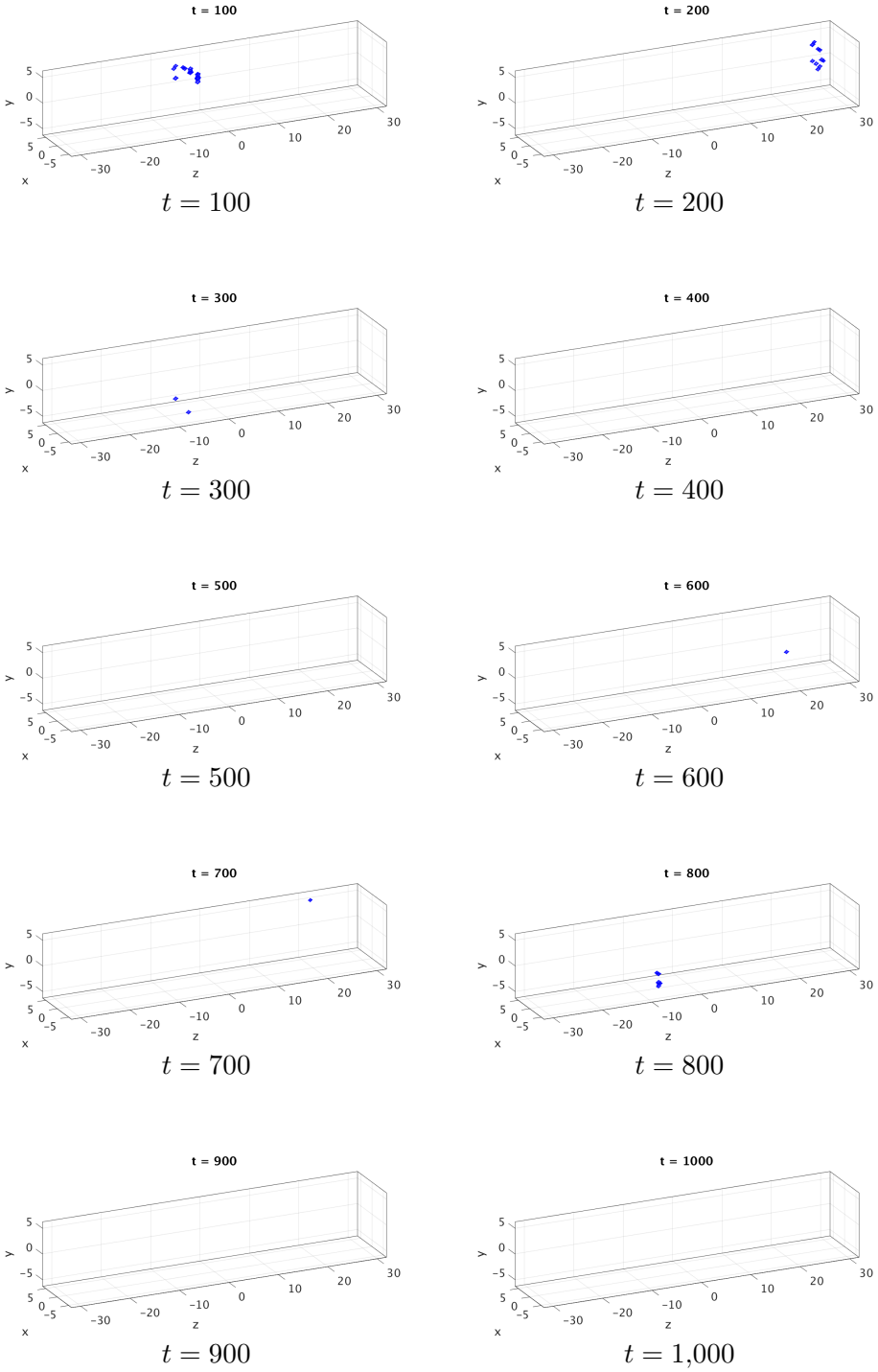

Figure 6.3: Concentration of $c(\mathbf{x}, t)$ throughout the cell for $\kappa = 0.1$, with a critical value of 65 μM.

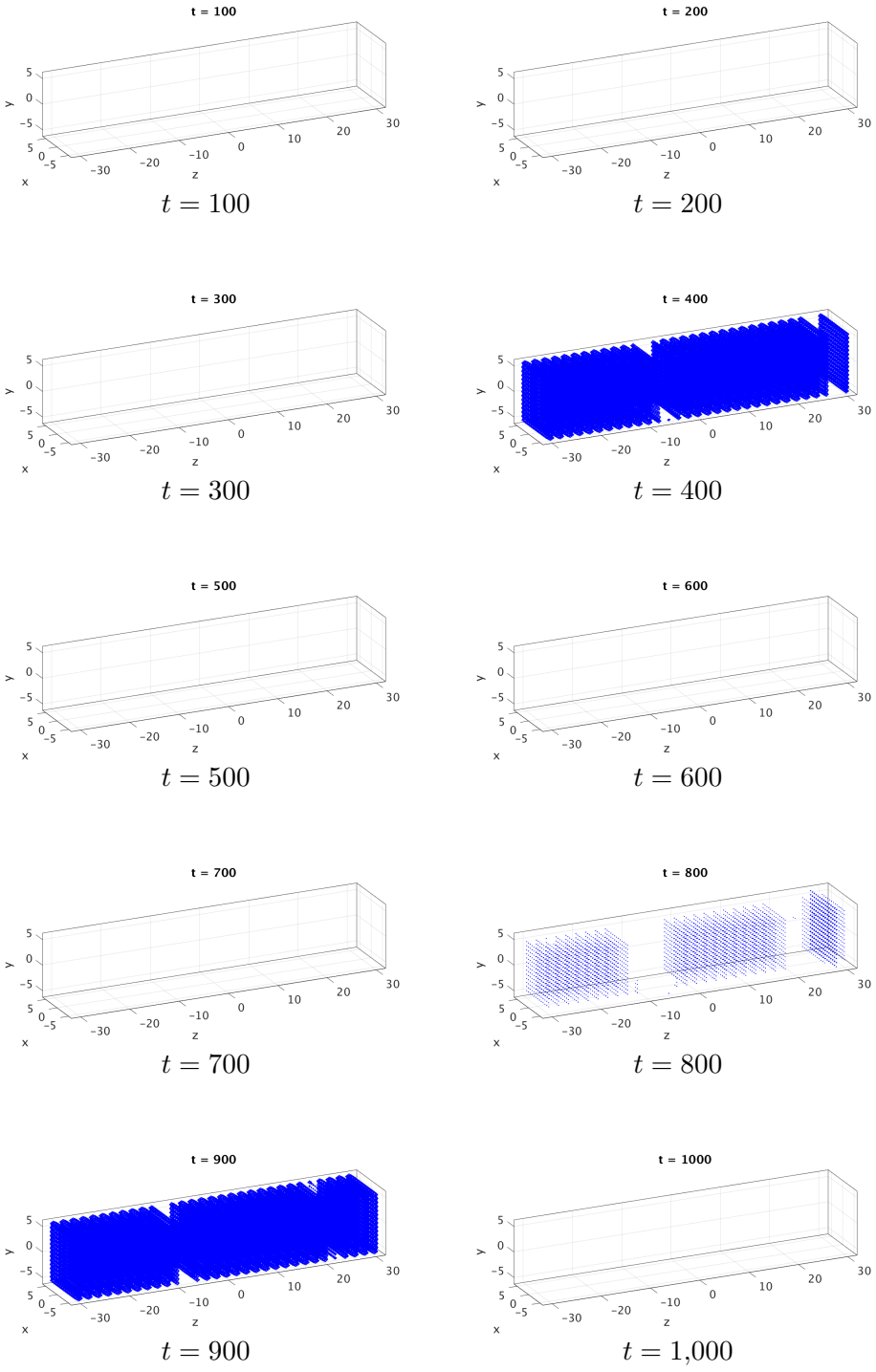

Figure 6.4: Concentration of ${b_1}^{(c)}(\mathbf{x}, t)$ throughout the cell for $\kappa = 0.1$, with a critical value of 46 μM.

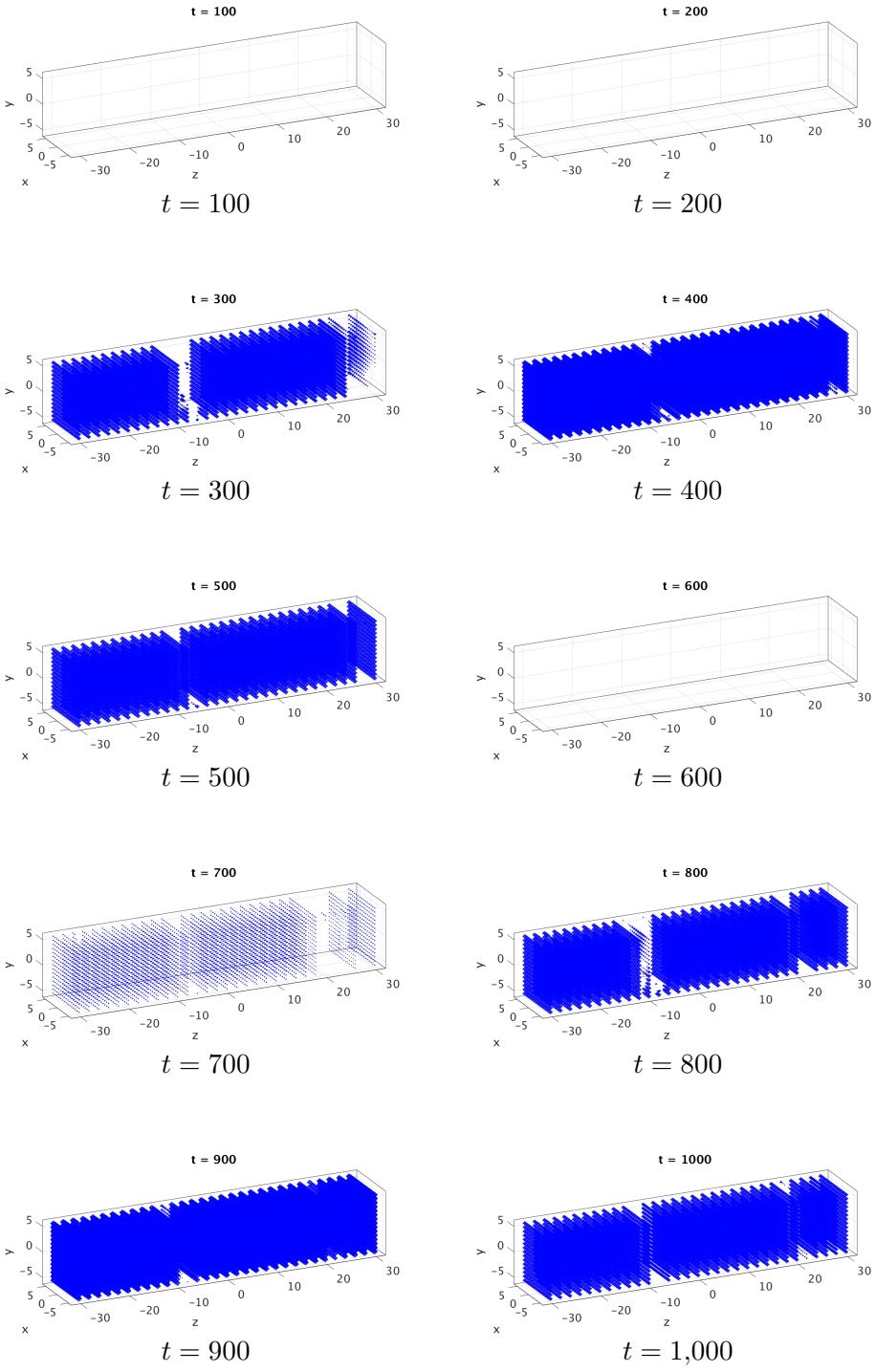

Figure 6.5: Concentration of ${b_2}^{(c)}(\mathbf{x}, t)$ throughout the cell for $\kappa = 0.1$, with a critical value of 112 μM .

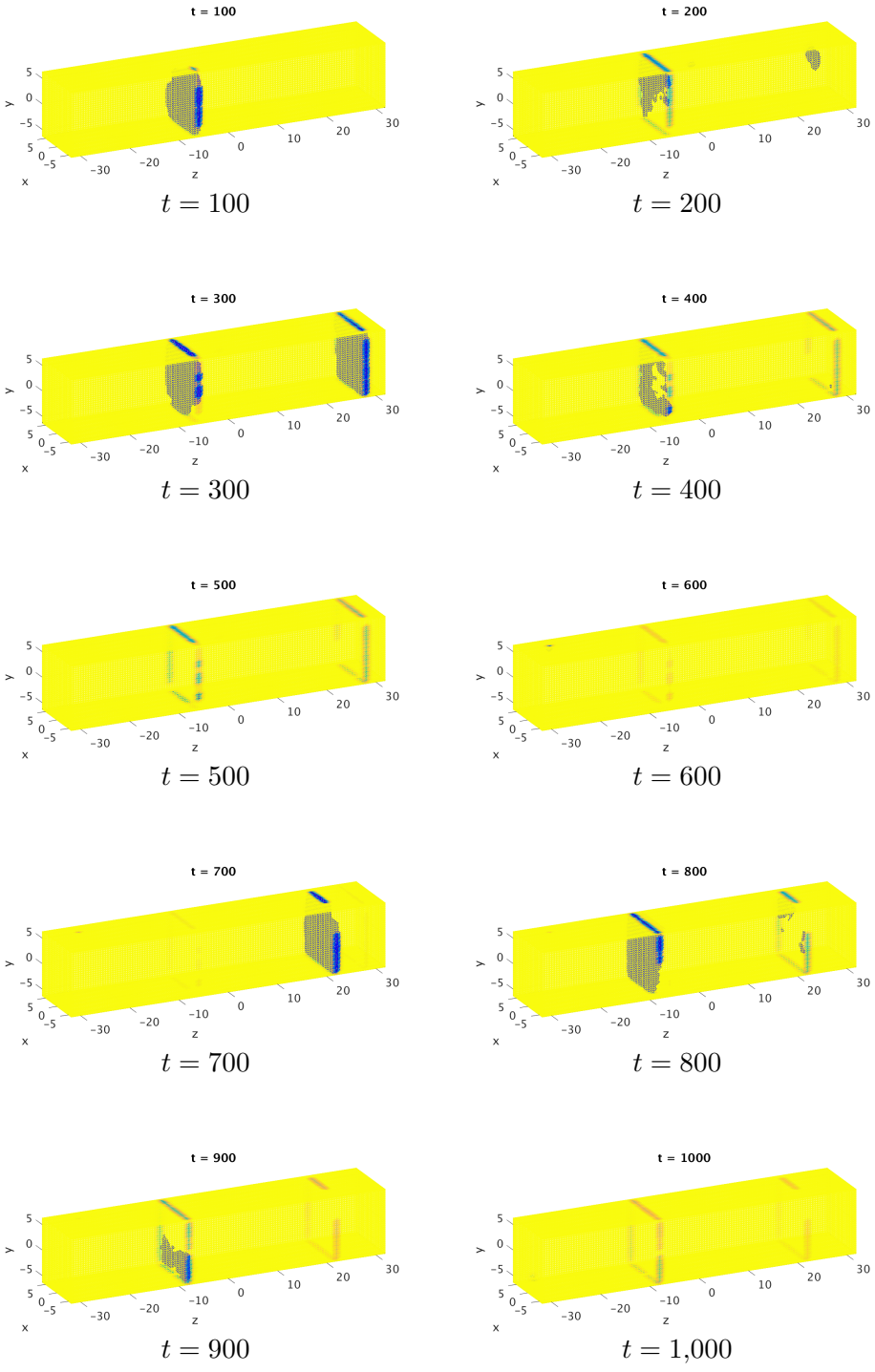

Figure 6.6: Concentration of ${b_3}^{(c)}(\mathbf{x}, t)$ throughout the cell for $\kappa = 0.1$, with a critical value of 120 μM.

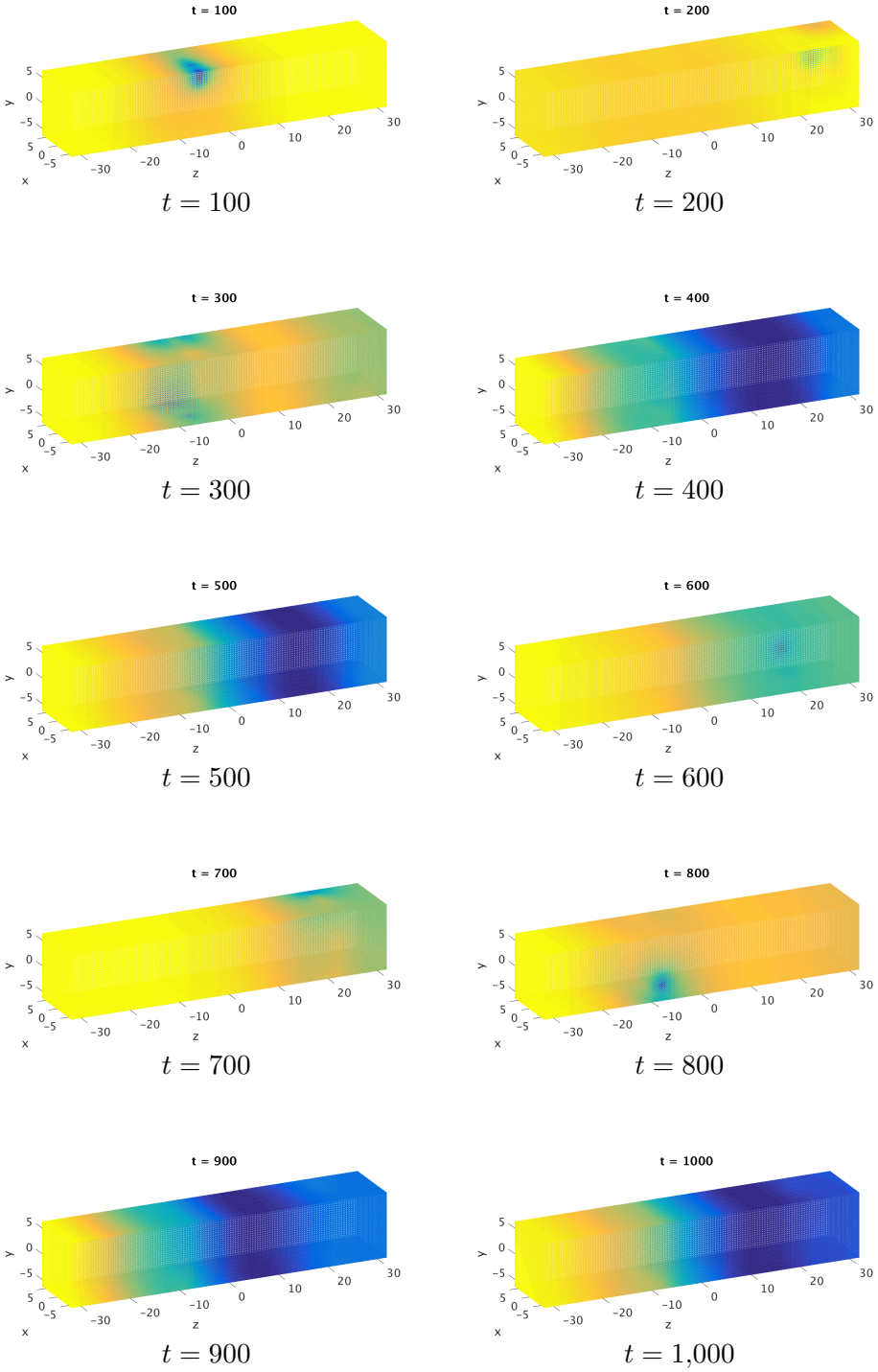

Figure 6.7: Concentration of $s(\mathbf{x}, t)$ throughout the cell for $\kappa = 0.1$, with a critical value of 5,000 μM.

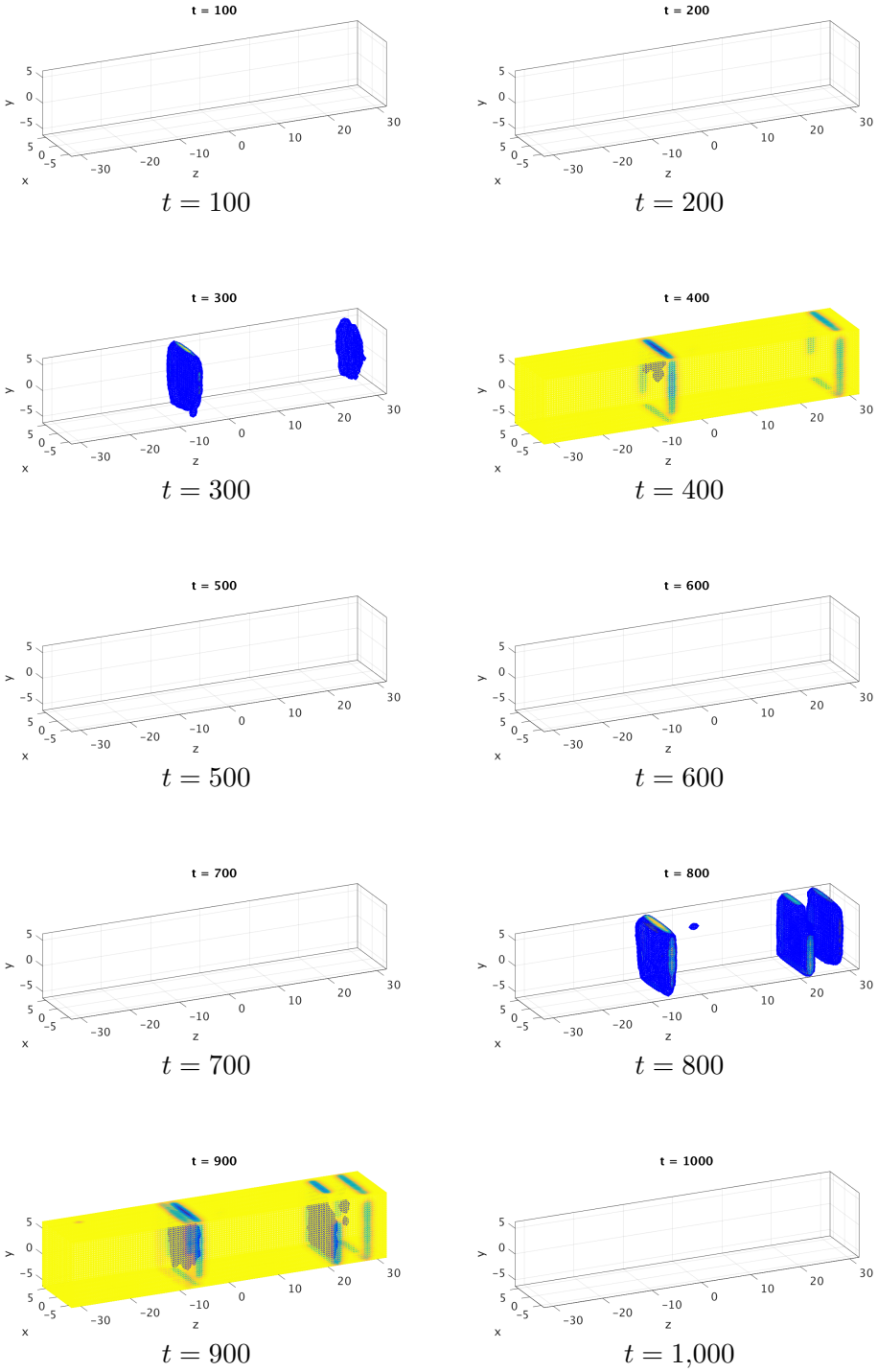

Figure 6.8: Concentration of $V(\mathbf{x}, t)$ throughout the cell for $\kappa = 0.1$, with a critical value of 0 mV.

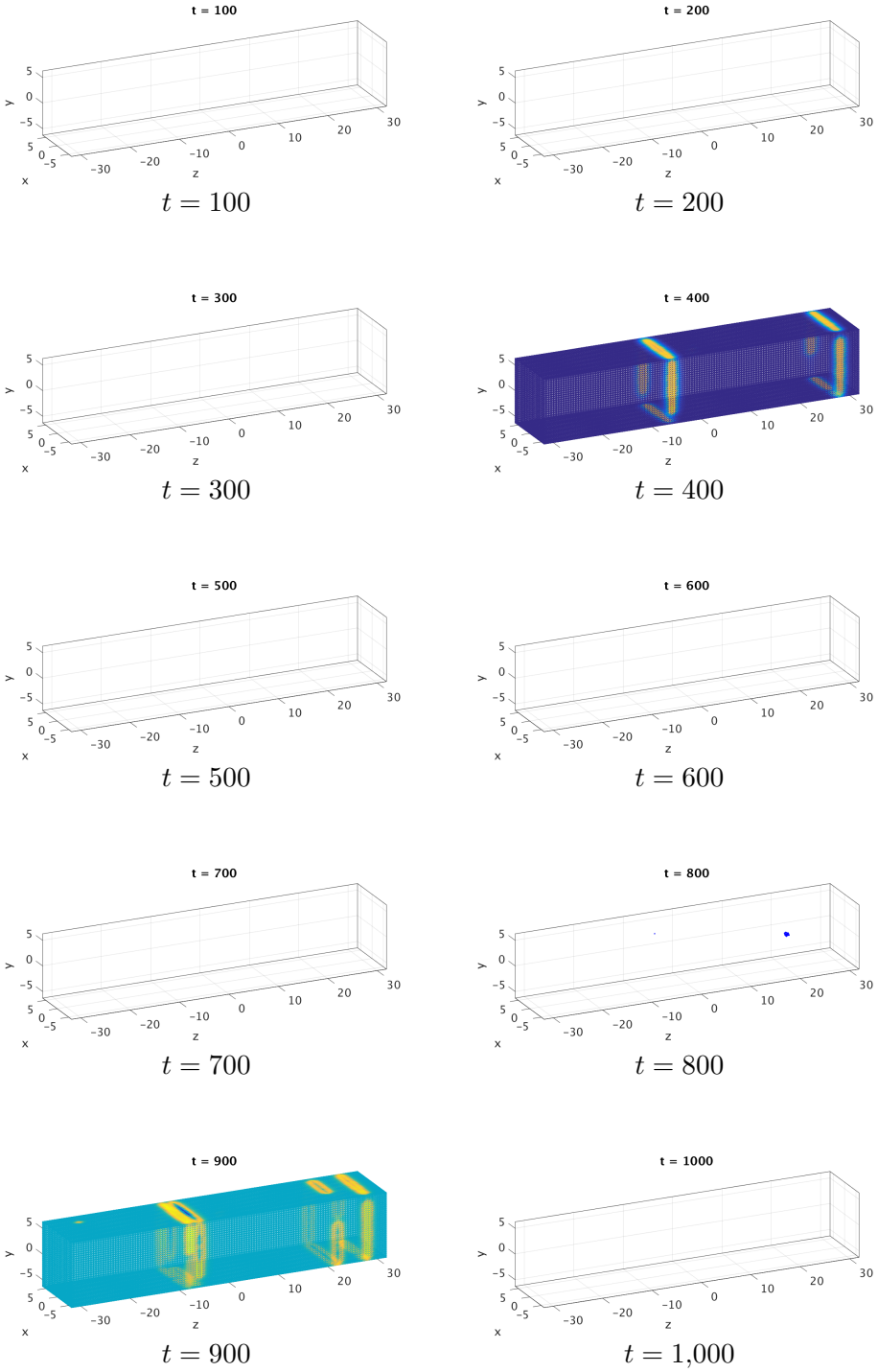

Figure 6.9: Concentration of $n(\mathbf{x}, t)$ throughout the cell for $\kappa = 0.1$, with a critical value of 0.3.

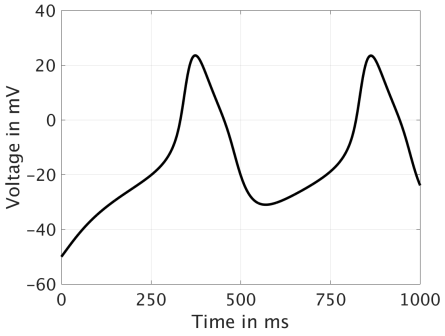

(a) Voltage over time.

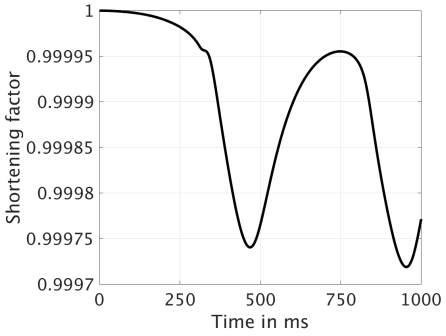

(b) Shortening factor over time.

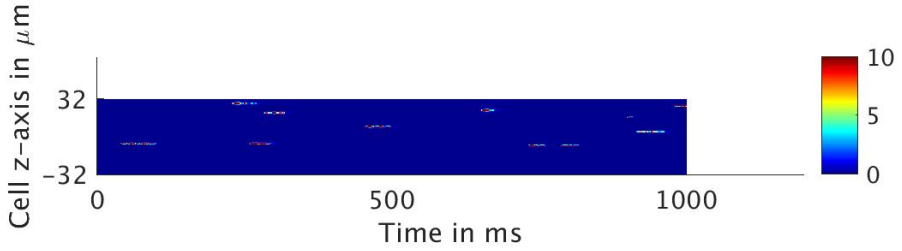

(c) Line scan.

Figure 6.10: Voltage, shortening factor, and line scan for $\kappa = 0.01$.

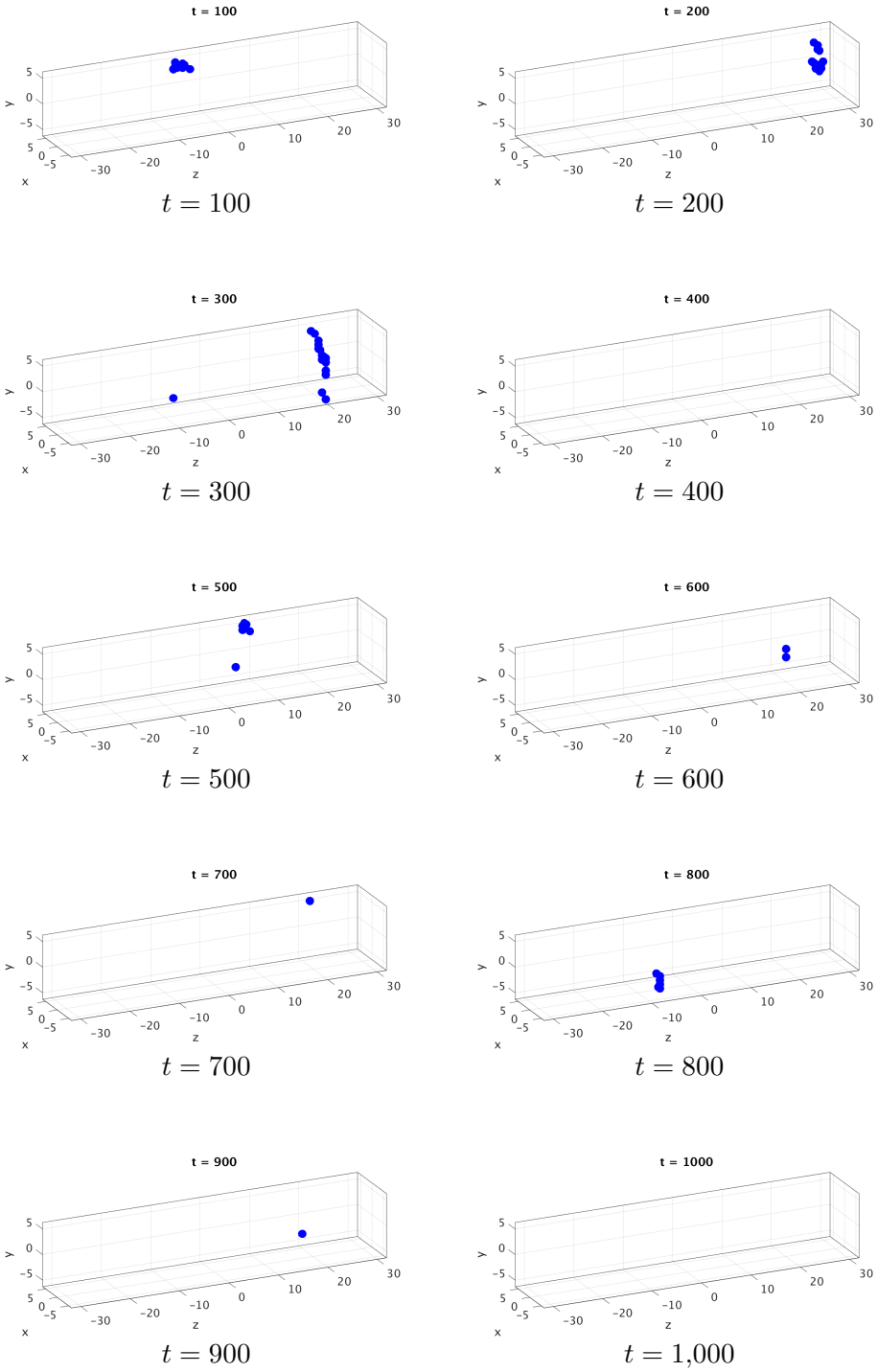

Figure 6.11: Open calcium release units throughout the cell for $\kappa = 0.01$.

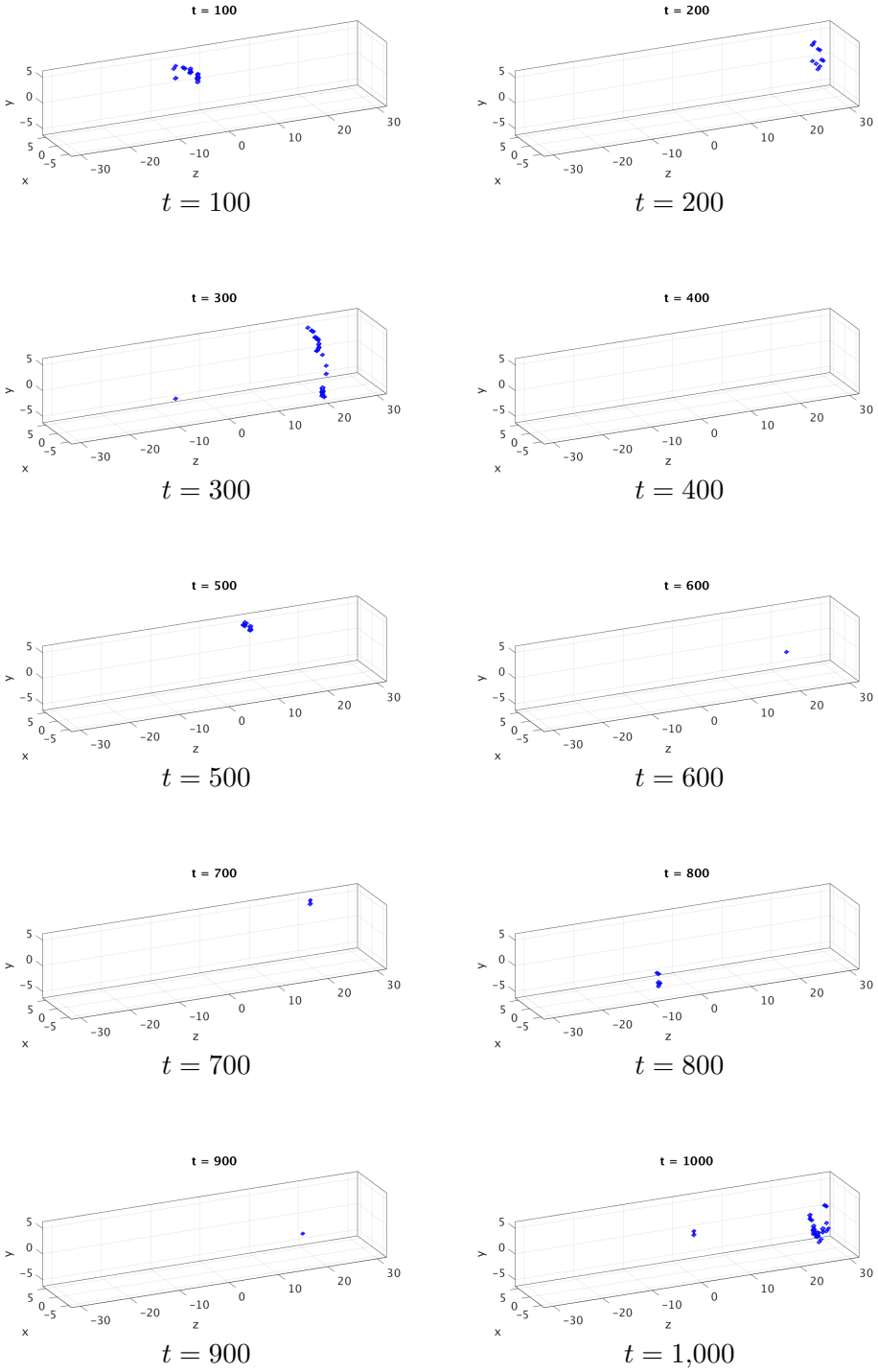

Figure 6.12: Concentration of $c(\mathbf{x}, t)$ throughout the cell for $\kappa = 0.01$, with a critical value of 65 μM.

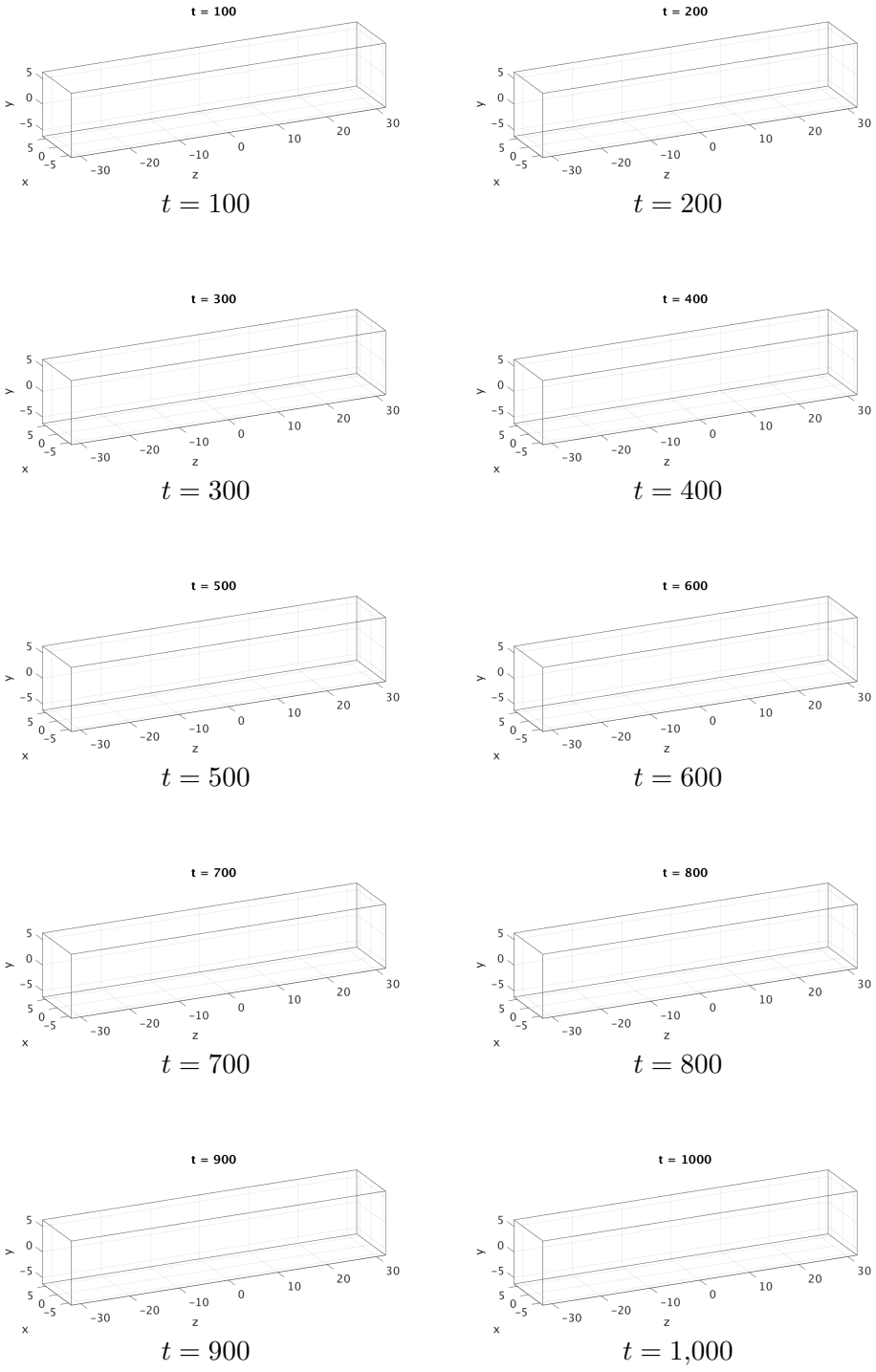

$t = 100$ $t = 200$

$t = 300$ $t = 400$

$t = 500$ $t = 600$

$t = 700$ $t = 800$

$t = 900$ $t = 1{,}000$

Figure 6.13: Concentration of ${b_1}^{(c)}(\mathbf{x}, t)$ throughout the cell for $\kappa = 0.01$, with a critical value of 46 μM.

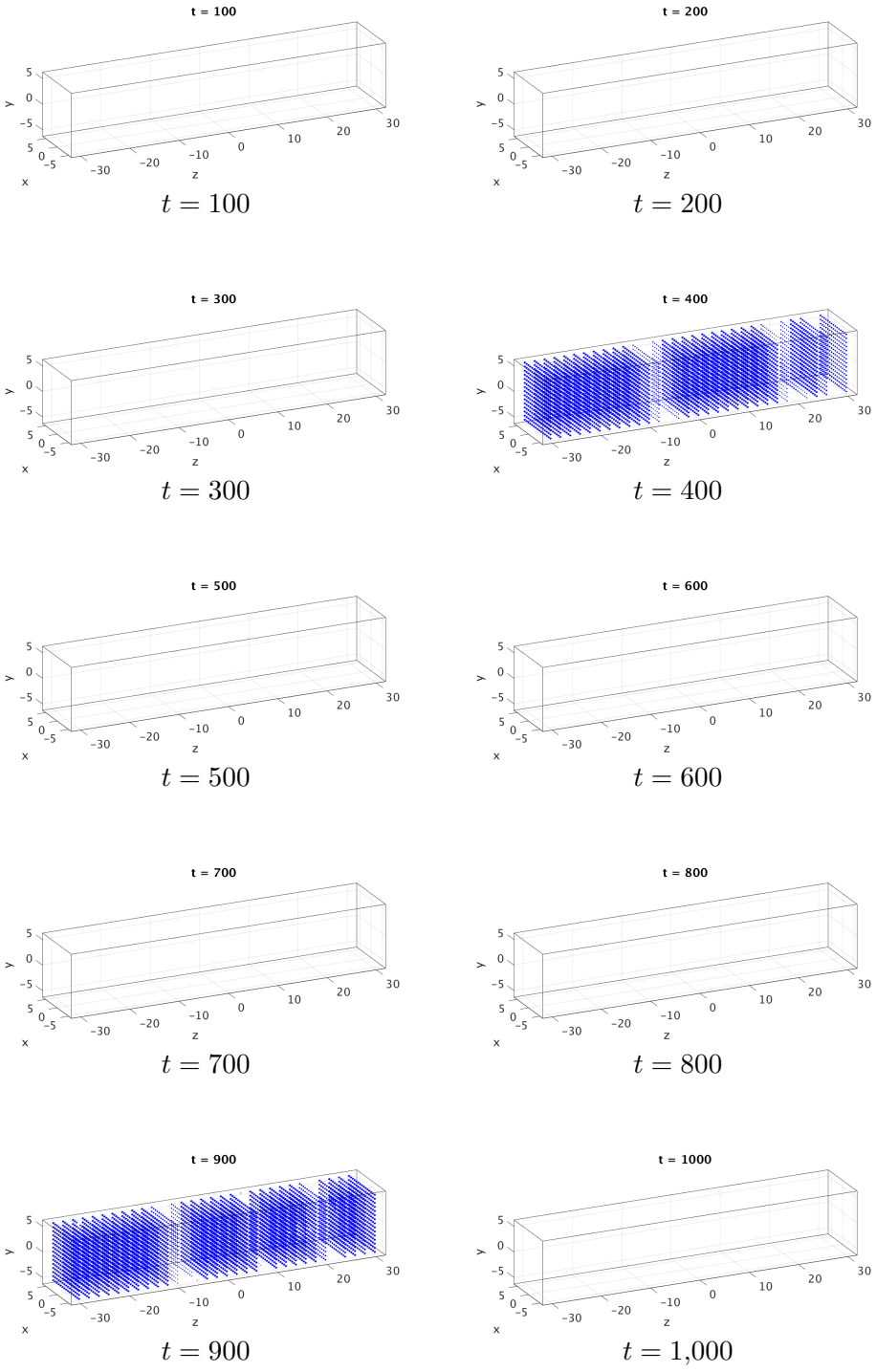

Figure 6.14: Concentration of ${b_2}^{(c)}(\mathbf{x}, t)$ throughout the cell for $\kappa = 0.01$, with a critical value of 112 μM .

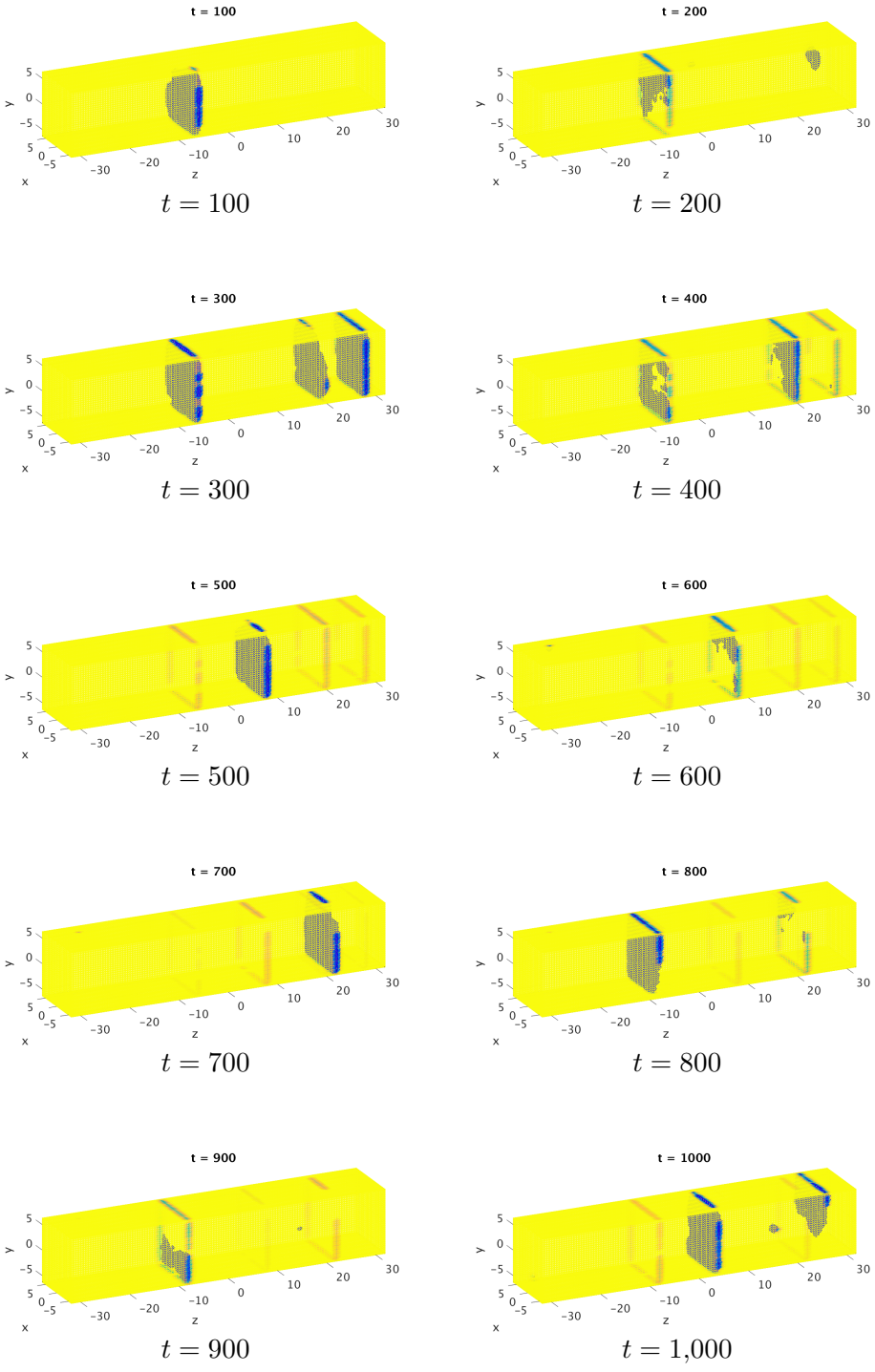

Figure 6.15: Concentration of ${b_3}^{(c)}(\mathbf{x}, t)$ throughout the cell for $\kappa = 0.01$, with a critical value of 120 μM.

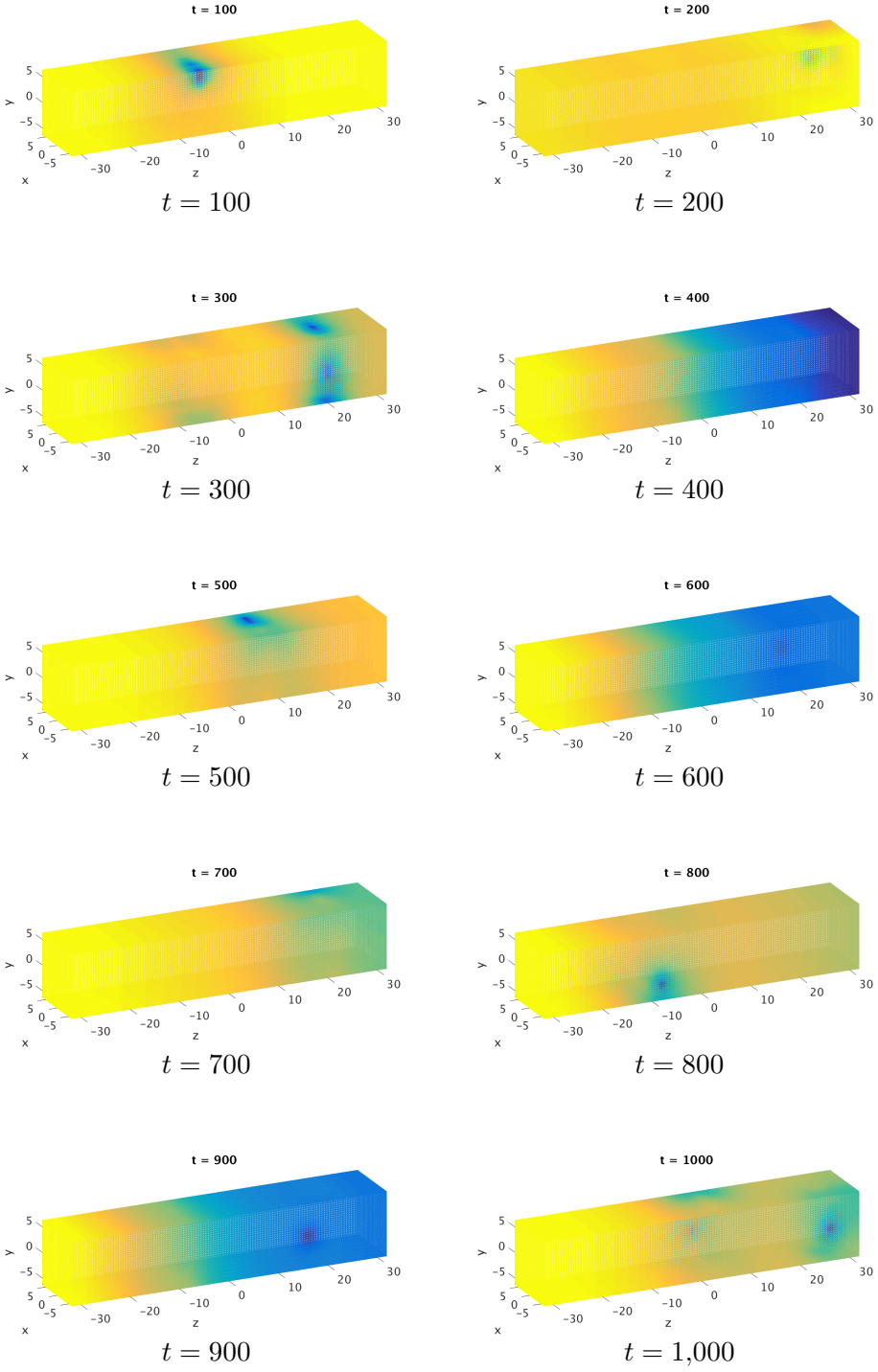

Figure 6.16: Concentration of $s(\mathbf{x}, t)$ throughout the cell for $\kappa = 0.01$, with a critical value of 5,000 μM.

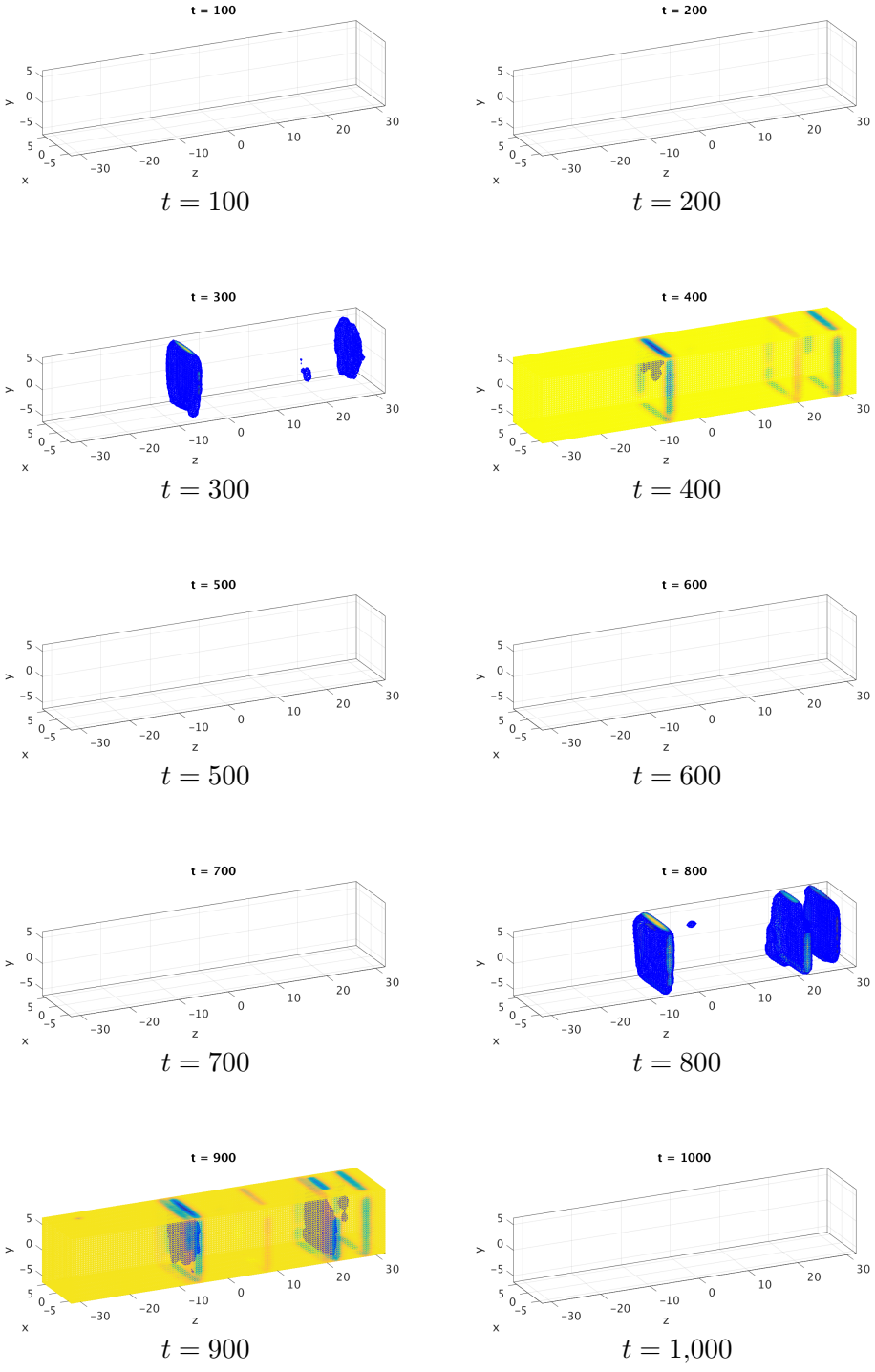

Figure 6.17: Concentration of $V(\mathbf{x}, t)$ throughout the cell for $\kappa = 0.01$, with a critical value of 0 mV.

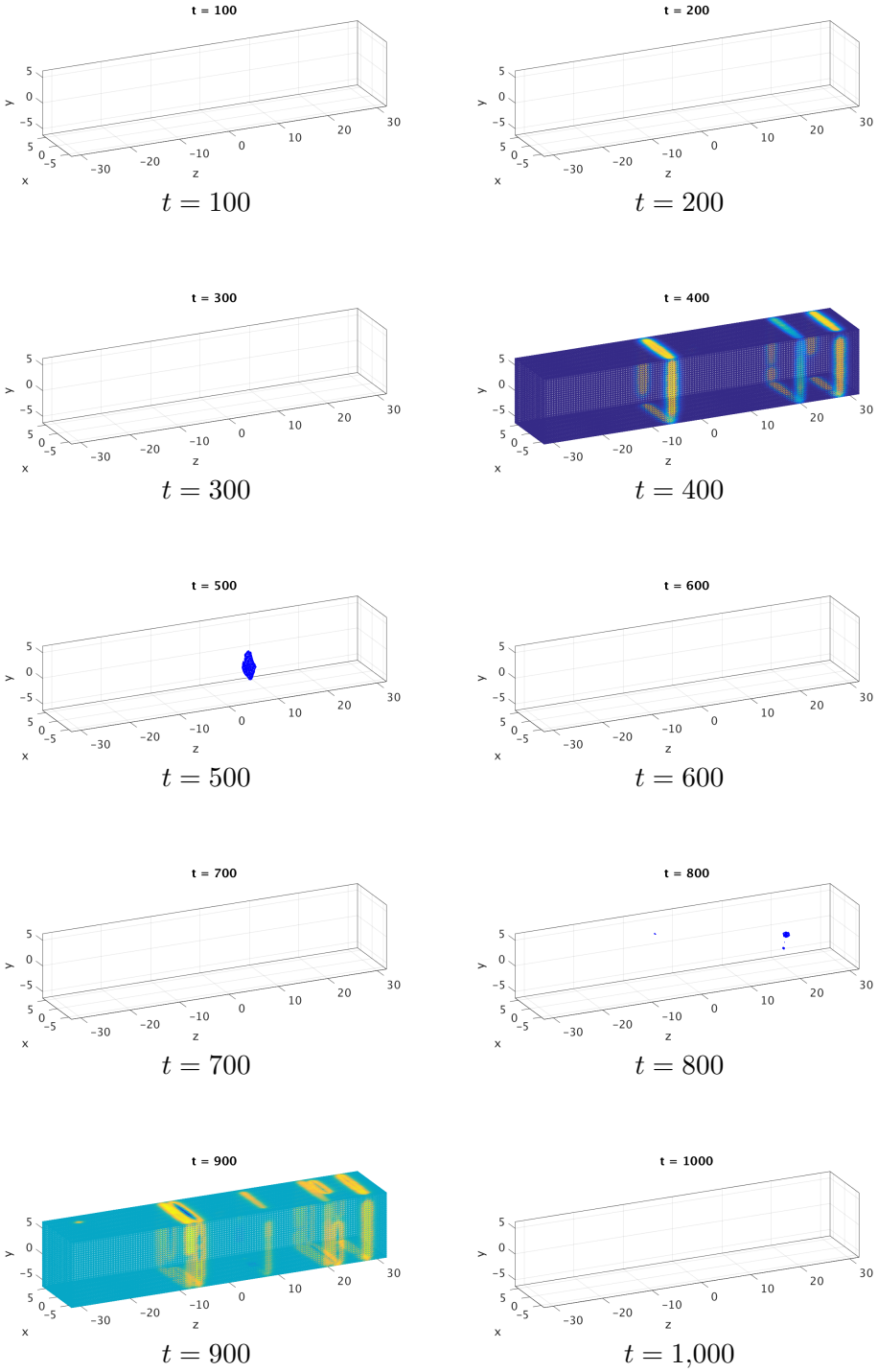

Figure 6.18: Concentration of $n(\mathbf{x}, t)$ throughout the cell for $\kappa = 0.01$, with a critical value of 0.3.

7 Conclusions

We now have a working seven variable model which includes for the first time the mechanical component of the excitation-contraction coupling (ECC) cycle in a heart cell. Our research included the successful implementation of the third cytosol buffer species, the inactive actin-myosin cross-bridges, and the links ③ and ④ in Figure 1.1. We simulated specific cases of coupling strength κ from the electrical to the calcium system to get a better understanding of the behavior of the model. From the results we notice that while modifying the κ value does not affect voltage significantly, it impacts many of the other species in the model including the cell's contraction. This is clear as we see differences in the plots of the shortening factor for the different sets of model parameters. The plots show that the contraction behavior mirrors that of the voltage and shows a realistic representation of what is physiologically happening. This report includes a documentation of the code design and specifically our differentiation of Jacobian matrix of the non-linear terms to show the careful development of the code. The Jacobian matrix is necessary for the non-linear Newton method, which in turn is required in the time-stepping method because of the stiffness of the ODE system that is created when the finite volume method is applied to the system of parabolic PDEs.

Because the plots of the shortening factor are not ideal to our understanding, future research done on this topic should include further parameter studies in order to get more reasonable behavior of the cell contraction. Once this is established, the model can be extended to include the eighth variable already proposed in [1, 2].

Acknowledgments

These results were obtained as part of the REU Site: Interdisciplinary Program in High Performance Computing (hpcreu.umbc.edu) in the Department of Mathematics and Statistics at the University of Maryland, Baltimore County (UMBC) in Summer 2017. This program is funded by the National Science Foundation (NSF), the National Security Agency (NSA), and the Department of Defense (DOD), with additional support from UMBC, the Department of Mathematics and Statistics, the Center for Interdisciplinary Research and Consulting (CIRC), and the UMBC High Performance Computing Facility (HPCF). HPCF is supported by the U.S. National Science Foundation through the MRI program (grant nos. CNS–0821258 and CNS–1228778) and the SCREMS program (grant no. DMS–0821311), with additional substantial support from UMBC. Co-authors Nygel Foster, and Darius Leftwich were supported, in part, by the UMBC National Security Agency (NSA) Scholars Program through a contract with the NSA. The team also thanks Wesley Collins for initial help with the cluster maya in HPCF. Graduate assistant Carlos Barajas was supported by UMBC. All of us thank Dr. Brad Peercy for invaluable discussions on the background and goals of mathematical physiology.

References

[1] Amanda M. Alexander, Erin K. DeNardo, Eric Frazier III, Michael McCauley, Nicholas Rojina, Zana Coulibaly, Bradford E. Peercy, and Leighton T. Izu. Impact of calcium store overload on electrical dynamics of cardiac myocytes. Technical Report HPCF–2015–25, UMBC High Performance Computing Facility, University of Maryland, Baltimore County, 2015.

[2] Amanda M. Alexander, Erin K. DeNardo, Eric Frazier III, Michael McCauley, Nicholas Rojina, Zana Coulibaly, Bradford E. Peercy, and Leighton T. Izu. Spontaneous calcium release in car-

diac myocytes: Store overload and electrical dynamics. *Spora: A Journal of Biomathematics*, 1, 2015.

[3] Kallista Angeloff, Carlos Barajas, Alexander D. Middleton, Uchenna Osia, Jonathan S. Graf, Matthias K. Gobbert, and Zana Coulibaly. Examining the effect of introducing a link from electrical excitation to calcium dynamics in a cardiomyocyte. *Spora: A Journal of Biomathematics*, 2, 2016.

[4] Kallista Angeloff, Carlos Barajas, Alexander D. Middleton, Uchenna Osia, Jonathan S. Graf, Matthias K. Gobbert, and Zana Coulibaly. Modeling the links between the chemical, electrical, and contractile calcium dynamics in a heart cell. Technical Report HPCF–2015–15, UMBC High Performance Computing Facility, University of Maryland, Baltimore County, 2016.

[5] Tamas Banyasz, Balazs Horvath, Zhong Jian, Leighton T Izu, and Ye Chen-Izu. Profile of L-type Ca 2+ current and Na+/Ca 2+ exchange current during cardiac action potential in ventricular myocytes. *Heart Rhythm*, 9(1):134–142, 2012.

[6] Xuan Huang, Matthias K. Gobbert, Bradford E. Peercy, Stefan Kopecz, Philipp Birken, and Andreas Meister. Order investigation of scalable memory-efficient finite volume methods for parabolic advection-diffusion-reaction equations with point sources, In preparation (2017).

[7] Leighton T. Izu, Joseph R. H. Mauban, C. William Balke, and W. Gil Wier. Large currents generate cardiac Ca^{2+} sparks. *Biophys. J.*, 80:88–102, 2001.

[8] Leighton T. Izu, Shawn A. Means, John N. Shadid, Ye Chen-Izu, and C. William Balke. Interplay of ryanodine receptor distribution and calcium dynamics. *Biophys. J.*, 91:95–112, 2006.

[9] Leighton T. Izu, W. Gil Wier, and C. William Balke. Evolution of cardiac calcium waves from stochastic calcium sparks. *Biophys. J.*, 80:103–120, 2001.

[10] Catherine Morris and Harold Lecar. Voltage oscillations in the barnacle giant muscle fiber. *Biophys. J.*, 35(1):193, 1981.

[11] Benjamin Mozaffarian et al. Heart disease and stroke statistics — 2015 update: A report from the american heart association. *Circulation*, 131(4):e29, 2014.

[12] Jonas Schäfer, Xuan Huang, Stefan Kopecz, Philipp Birken, Matthias K. Gobbert, and Andreas Meister. A memory-efficient finite volume method for advection-diffusion-reaction systems with non-smooth sources. *Numer. Methods Partial Differential Equations*, 31(1):143–167, 2015.